AD-A194 562 RADIAL MIXING IN TURBOMACHINES(U) VRIJE UNIV BRUSSELS (BELGIUM) DEPT OF FLUID MECHANICS J DENUYCK ET AL. 01 FEB 88 VUB-TN-40 AFOSR-TR-88-0421 AFOSR-85-0167 1/1

UNCLASSIFIED F/G 20/4 NL

END
DATE FILMED
8 88

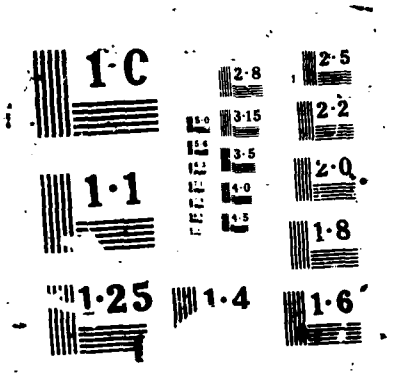
1·C
1·1
1·25
1·4
2·8
3·15
3·5
4·0
4·5
2·5
2·2
2·0
1·8
1·6

Grant N° AFOSR-85-0167

RADIAL MIXING IN TURBOMACHINES

by

DE RUYCK J., HIRSCH CH.

Dept. of Fluid Mechanics
Vrije Universiteit Brussel
Pleinlaan 2, 1050 Brussels
Belgium

February 1, 1988

Final scientific report
September 1, 1985 - August 31, 1987
VUB-TN-40

Approved for public release, distribution unlimited

- Prepared for -

Air Force Office for Scientific Research
Bolling AFB, USA

and

European Office of Aerospace Research and Development
London, England

UNCLASSIFIED

SECURITY CLASSIFICATION OF THIS PAGE

REPORT DOCUMENTATION PAGE

1a. REPORT SECURITY CLASSIFICATION: Unclassified	1b. RESTRICTIVE MARKINGS
2a. SECURITY CLASSIFICATION AUTHORITY	3. DISTRIBUTION/AVAILABILITY OF REPORT: Approved for public release; Distribution unlimited
2b. DECLASSIFICATION/DOWNGRADING SCHEDULE	
4. PERFORMING ORGANIZATION REPORT NUMBER(S): VUB-TN- 40	5. MONITORING ORGANIZATION REPORT NUMBER(S): AFOSR-TR- 88-0421
6a. NAME OF PERFORMING ORGANIZATION: Vrije Universiteit Brussel, Dept. of Fluid Mechanics; 6b. OFFICE SYMBOL (If applicable): VUB-STRO	7a. NAME OF MONITORING ORGANIZATION: European office for Aerospace Research and Development
6c. ADDRESS (City, State and ZIP Code): Pleinlaan 2, 1050 BRUSSELS BELGIUM	7b. ADDRESS (City, State and ZIP Code): Marylebone Road, LONDON ENGLAND
8a. NAME OF FUNDING/SPONSORING ORGANIZATION: Air Force Office for Scientific Research; 8b. OFFICE SYMBOL (If applicable): AFOSR/NA	9. PROCUREMENT INSTRUMENT IDENTIFICATION NUMBER: AFOSR-85-0167
8c. ADDRESS (City, State and ZIP Code): Building 410 Bolling AFBDC, 20332-6448 USA	10. SOURCE OF FUNDING NOS.

PROGRAM ELEMENT NO.	PROJECT NO.	TASK NO.	WORK UNIT NO.
61102F	2307	S1	

11. TITLE (Include Security Classification): Radial mixing in Turbomachines

12. PERSONAL AUTHOR(S): De Ruyck J. Hirsch Ch.

13a. TYPE OF REPORT	13b. TIME COVERED	14. DATE OF REPORT (Yr., Mo., Day)	15. PAGE COUNT
FINAL	FROM 85-9-1 TO 87-8-31	88-2-1	68

16. SUPPLEMENTARY NOTATION

17. COSATI CODES			18. SUBJECT TERMS (Continue on reverse if necessary and identify by block number)
FIELD	GROUP	SUB. GR.	Radial Mixing Secondary flow Wakes

19. ABSTRACT: A radial mixing calculation method is presented where both convective and turbulent mixing processes are included. The secondary flows needed for the convective mixing are derived from pitch averaged vorticity equations combined with integral methods for the 3D end-wall boundary layers, 3D profile boundary layers and 3D asymmetric wakes. The convective transport due to secondary flows is computed explicitly. The method is applied to a cascade and two single stage rotors. The three test cases show a very different secondary flow behaviour which allows the analysis of the relative importance of the different secondary flow effects. Turbulent diffusion is found to be the most important mixing mechanism, whereas convective mixing becomes significant when overall radial velocities exceed about 5% of the main velocities. The wake diffusion coefficient is found to be representative for the turbulent radial mixing and is the only empirical constant to be determined.

20. DISTRIBUTION/AVAILABILITY OF ABSTRACT	21. ABSTRACT SECURITY CLASSIFICATION
UNCLASSIFIED/UNLIMITED ☒ SAME AS RPT. ☒ DTIC USERS ☐	Unclassified

22a. NAME OF RESPONSIBLE INDIVIDUAL	22b. TELEPHONE NUMBER (Include Area Code)	22c. OFFICE SYMBOL
H.E. HEUN	202 767 0471	AFOSR/NA

DD FORM 1473, 83 APR EDITION OF 1 JAN 73 IS OBSOLETE.

Unclassified

SECURITY CLASSIFICATION OF THIS PAGE

Grant Nº AFOSR-85-0167

RADIAL MIXING IN TURBOMACHINES

by

DE RUYCK J., HIRSCH CH.

Dept. of Fluid Mechanics
Vrije Universiteit Brussel
Pleinlaan 2, 1050 Brussels
Belgium

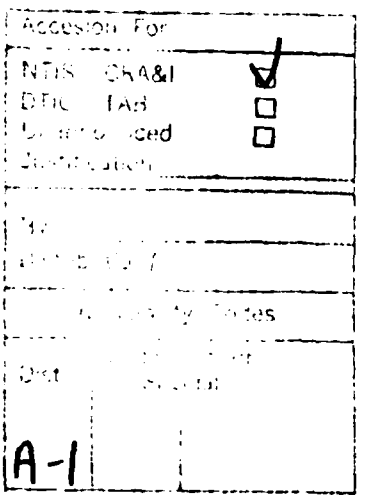

February 1, 1988

Final scientific report
September 1, 1985 - August 31, 1987
VUB-TN-40

Approved for public release, distribution unlimited

- Prepared for -

Air Force Office for Scientific Research
Bolling AFB, USA

and

European Office of Aerospace Research and Development
London, England

CONTENTS

NOMENCLATURE

b boundary layer parameter

C_f friction coefficient

c absolute velocity component, chord

E entrainment rate

F force defect thickness

f blade force, wake model function (eq 9.3)

g wake model function (eq 9.4)

H shape factor

H^* Head's shape factor

h annulus height, metric coefficient

m meridional coordinate

n coordinate normal to the end-walls

p static pressure

R_{ij} radii of curvature (appendix A)

r radius, recovery factor

s streamwise coordinate, pitch

T temperature

T_t total temperature

t transverse coordinate

t_c tip clearance

U wheel speed

u pitchwise coordinate

W velocity in the blade reference system

w relative velocity component

z axial coordinate

α radial flow angle

β passage flow angle

γ stagger angle

δ physical boundary layer thickness

δ^* displacement thickness

ϵ skewing angle, diffusion coefficient

ϵ_w wall skewing angle

η u/δ

θ momentum thickness, angular coordinate

λ correction momentum thickness

ν viscosity, eddy viscosity

ρ density

σ solidity, wall inclination angle (fig A.3)

τ shear stress

ω vorticity vector

Subscripts

w at the wall

m,n,u in meridional coordinates (fig. A.3)

s,n,t in streamline coordinates

sec secondary flow

ewbl end-wall boundary layer

inv inviscid

Superscripts

$\hat{}$ inviscid flow parameter

$\tilde{}$ passage-averaged value

Abbreviations

EWBL end-wall boundary layer

PBL profile boundary layer

3D three-dimensional

1. INTRODUCTION

The design requirements for axial compressors have increased considerably during the last twenty years, calling for more advanced computational methods. However, the high complexity of the flow pattern prevents full three-dimensional calculations in multistage configurations. The flow is therefore computed by parts which interact with each other.

The current approach consists in the splitting of the turbomachine flow into two two-dimensional flows (Hirsch and Warzee, 1979). The first flow is considered in a circumferential blade-to-blade surface (S1) and the second is the circumferentially averaged meridional flow (S2). Different secondary effects which are not considered in these S1 and S2 flows are to be computed separately and superposed in an interactive way. The trend towards higher stage loadings and lower aspect ratio's enhances the effect of radial redistributions which are not considered in current axisymmetric calculation methods. Adkins and Smith (1982) presented a basic formulation for the determination of radial mixing effects, where the secondary flows are found from a classical inviscid approach (figure 1.1). The effects of end-wall boundary layers, blade tip clearances and blade radial flows are introduced in a simplified way based on empirical information. The radial mixing is expressed through a diffusion type equation where the 'diffusion' or 'mixing' coefficient is a function of the rms radial velocity. This formulation was further investigated by Whitfield and Keith (1985). Several applications show the importance and the correct behaviour of this mixing theory. Gallimore and Cumpsty (1986), and later Wisler et al. (1987) showed that mixing due to turbulent diffusion is at least as important as mixing due to radial convection and an additional turbulent mixing coefficient is to be considered.

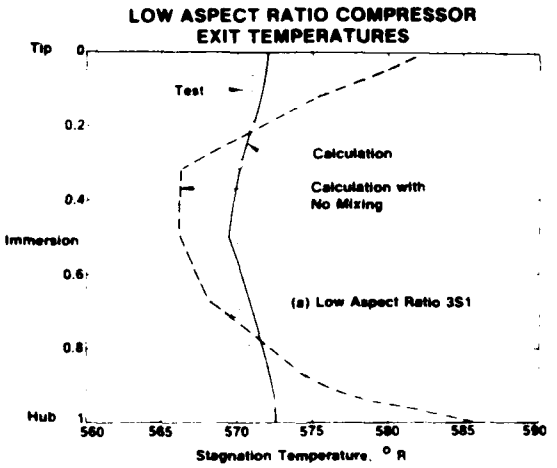

Figure 1.1 : Radial redistribution of total temperature (Adkins and Smith, 1982)

The above approaches are validaded by experiments, although the mechanisms they use are very different. This validation is obtained through the calibration of empirical constants, which compensates the possible shortcomings of these approaches. A shortcoming of the Adkins and Smith approach is certainly that a convection process may behave in a way strongly different from a diffusion mechanism. As an example, a flow with a constant radial temperature gradient is not directly affected by a diffusion process, since the radial second temperature derivative is zero. The radial flow

migrations may however affect this gradient in a significant way. In the present work, the convective mixing is found from the passage averaged secondary vorticity, coupled to the radial flow components obtained from integral boundary layer and wake predictions. A new mixing procedure based on the explicit computation of the full transport equation is proposed. This full computation makes the simulation of tracer gas injection experiments possible.

2. HISTORICAL BACKGROUND

The present section reviews briefly the secondary flow and radial mixing theories. The different secondary flows present in a compressor passage are summarised on figure 2.1 and are discussed separately in sections 2.1 to 2.6. Two different approaches for the determination of the secondary flows are given in section 2.7, section 2.8 discusses radial mixing processes and section 2.9 is a brief review of experimental work in this field.

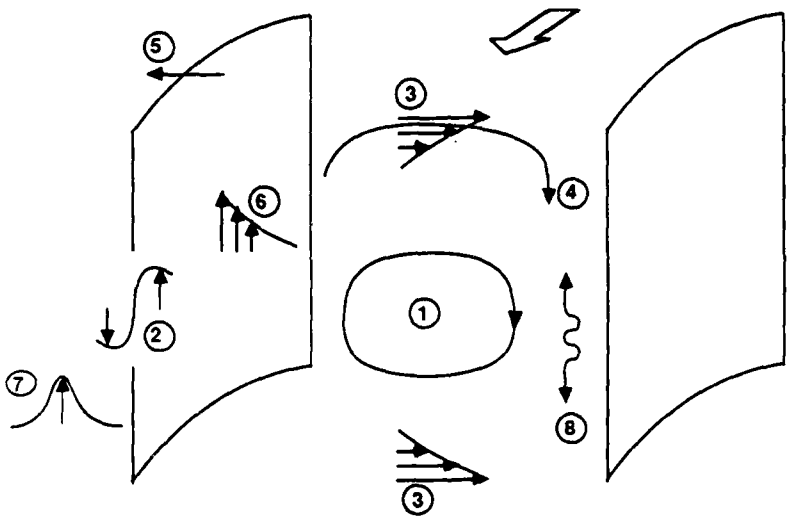

Flow :	Origin :
1 Main passage vortex	Flow non-uniformities
2 Trailing shed and filament vortex	Spanwise changes in circulation
3 End wall boundary cross flow	Boundary layer overturning
4 End wall b. l. passage vortex	Boundary layer overturning
5 Tip clearance flow	Tip clearance pressure difference
6 Profile boundary layer radial flow	Centrifugation
7 Wake radial flow	Centrifugation
8 Radial diffusion	Turbulence

Figure 2.1 : Secondary flows

2.1 Passage vortex (contributions 1,3,4)

The passage vortex is a well known secondary flow component in turbomachine flows. Its mechanism has been investigated a first time by Carter and Cohen (1946) for uniform flows with thin boundary layers and by Squire and Winter (1951) for nonuniform flows. It was further investigated by Hawthorne (1951) and A.G. Smith (1957) for cascades and by Dixon (1974) for rotating blade rows.

The passage vortex is basically a streamwise vorticity component caused by the deflection of a non-uniform mainstream velocity. It can be obtained from the conservation of momentum in a steady, inviscid incompressible fluid (Carter and Cohen, 1946, Squire and Winter, 1951)

$$\vec{\nabla} \wedge (\vec{W} \wedge \vec{\omega}) = 0 \qquad (2.1)$$

The inviscid equation (2.1) is often applied over the whole passage, including the viscous boundary layers. In a different approach (see 2.7), the flow is considered as a superposition of (i) a main inviscid primary flow, and (ii) viscous boundary layer flows which are treated through integral boundary layer methods. In the latter case, a distinction is to be made between a 'main passage vortex' caused by an overall non-uniform inlet flow as predicted by a through-flow computation, and an 'end-wall boundary layer passage vortex'.

2.2 Trailing edge vorticity (contribution 2)

The vortex sheet leaving the trailing edge of the blade has two components : the trailing filament and the trailing shed vorticities. The shed vorticity is due to the changes in circulation along the span, the filament vorticity is due to the stretching of vortex filaments and is a result of non-uniformities in the inlet flow. Circulation changes can be due either to an overall non-free vortex behaviour of the passage flow, either to specific changes in blade loading inside the end-wall boundary layers.

These components were investigated a first time by Hawthorne (1955) and Came and Marsh (1974) on the basis of inviscid flow models.

2.3 Tip clearance flows (contribution 5)

Tip clearance flows contribute to the secondary flow motion in an important way. They affect the passage vortex by modifying the flow turning and the trailing edge vortex through a change in blade loading. Smith (1955) proposed an inviscid approach where tip clearance and leakage secondary flows are taken into account. Several empirical constants were introduced. In an approach where boundary layers flows are considered separately, tip clearance effects can be included in the integral boundary layer equations (De Ruyck and Hirsch, 1983) (see 2.7).

2.4 Profile boundary layer radial flows (contribution 6)

Boundary layers along turbomachine blades are three dimensional and contribute to the radial convection. Both experimental and theoretical

information about these radial flows is poor. Adkins and Smith (1982) estimated these radial flows by solving the local conservation of radial momentum along the blade, introducing two empirical constants. The radial velocity was found to be a direct consequence of the boundary layer velocity gradient. Their development is inviscid, in the same way as was done for the passage vortex. Whitfield and Keith (1984) used the same base but included the blade loading effects by means of the loss correlations of Koch and Smith.

Viscous 3D boundary layer applications on turbomachine blades are almost inexistant. More experimental information has recently been made available by Laksminarayana and Popovski (1987).

2.5 Wake radial flows (contribution 7)

The wake can be considered as an important element in the total radial flow analysis. Peak values in radial velocity are observed in the near wake, where very low velocities may induce a high centrifugation. Adkins and Smith (1982) and Whitfield and Keith (1984) treated the wake by writing the mainstream and radial momentum conservation laws along the wake center. The total amount of radial flow is found by modeling the wake profiles. Since symmetric wake models are used, there is no ability to simulate asymmetric radial wake profiles. Hah and Lakshminarayana (1979) made full turbulent 3D computations in asymmetric wakes with radial flows. These computations are in good agreement with detailed experiments, but their cost may be in disproportion to the gain in useful information.

2.6 Radial diffusion (contribution 8)

All the above radial flows contribute to radial mixing by a convection mechanism. Gallimore and Cumpsty (1986a, 1986b) showed that at least in their test compressor the radial energy redistribution is due mainly to turbulent diffusion. They based their conclusion on the facts (i) that the observed mixing was isotropic and (ii) that the measured turbulent energy production is almost fully compensated by turbulent energy diffusion, which means that convection phenomena are of less importance.

2.7 Two approaches for secondary flows

From the the above discussion on secondary flows, it follows that a part of them originate in three viscous layers :

(i) the end-wall boundary layers
(ii) the profile boundary layers
(iii) the wakes

The cross flows in these layers may be estimated in two ways :

(i) solving local inviscid equations over the whole span, including the viscous layers
(ii) exclude the viscous layers from the inviscid solution and solving them separately by means of integral boundary layer and wake equations

The first approach has been referred to in sections 2.1 to 2.4. A large amount of such inviscid secondary flow approaches is reviewed in the AGARD conference proceedings 214 (1977) about 'Secondary Flows in Turbomachines.

In the integral boundary layer and wake approach, secondary flows are predicted in a less detailed way, whereas viscous effects can be taken into account. Secondary flows are characterised by some integral cross flow thicknesses which quantify a total amount of secondary mass and momentum flow.

Early 3D end-wall boundary layer (EWBL) equations were proposed by Cooke and Hall (1962) and Horlock (1971). Smith (1969) showed the presence of variations in blade loading inside the boundary layers, which can affect the secondary flow in an important way, and he showed the importance of the tip clearance effects. Mellor & Wood (1971) and Horlock & Perkins (1974) took these effects into account through the introduction of force defects. De Ruyck & Hirsch (1983) extended this theory by introducing (i) new correlations for the force defects and (ii) profile model equations suited for turbomachine EWBL flows, which allow the reconstruction of complete spanwise pitch averaged cross flow profiles. Only two empirical constants which are extensively calibrated are present in this method.

Detailed 3D profile boundary layer (PBL) and wake equations are less profuse and as a first step in the present project, 3D boundary layer and wake equations were developed in fully curvilinear coordinates. This development is applied in a coherent way for EWBL as well as PBL and wakes. Recent theoretical developments of full 3D boundary layer equations are summarised in an AGARD report on 'Computation of Three-Dimensional Boundary Layers Including Separation' report 741, 1986. This refence discusses the problem of separations, a problem which is not yet treated in the present report, but which is to be included in the future since it appears from the available test cases that the trailing edge separation plays an important role in the near wake, including the induction of radial flows.

Although inviscid theories are important for the understanding of secondary flows, these thheories are practically not applied in multistage design codes, except for radial flows along profiles and in wakes. The present proposal therefore seeks for a complete integral approach for the secondary flow description. Integral secondary flow results are next used as input for the description of the radial mixing process.

2.8 Radial mixing process

Adkins & Smith (1982) proposed a diffusion type mixing equation which can be applied for the mixing of any flow parameter. The 'diffusion' or 'mixing' coefficient is determined from the knowledge of the secondary flow, which in their case is obtained from Smith's inviscid secondary flow approach. Some of their applications show the importance and the correct behaviour of this mixing theory. More recently, Gallimore and Cumpsty (1986) presented much simpler computations based on the turbulent mixing only. Whitfield and Keith (1984) made a more clear distinction between convection and diffusion mechanisms. The did not consider the convection as being isotropic, as was done by Adkins through the use of a diffusion type equation. They rather traced the flow particles and obtained non-isotropic flow property migrations in the spanwise direction.

The three above approaches are validaded by experiments, although the mechanisms they use are very different. This validation is however obtained

through the calibration of empirical constants, which probably compensates the shortcomings of these approaches. In order to clarify this situation, one of the scopes of the present work will be to determine the relative importance of mixing through convection and mixing through turbulent diffusion. The diffusion type equation of Adkins & Smith will be applied in the present approach and any flow property ϕ will be radially redistributed through

$$\frac{\partial \phi}{\partial m} = \varepsilon \frac{\partial^2 \phi}{\partial n^2} \tag{2.2}$$

where, combining convection and diffusion,

$$\varepsilon = \int_{\text{pitch}} \frac{w_n^2}{w_m^2} \, d\theta + \text{turbulent diffusion coefficient} \tag{2.3}$$

w_m and w_n denote the meridional and radial velocities, θ the angular coordinate. Equation (2.2) does not include mixing losses, it only expresses the mixing process. It can easily be solved through a numerical scheme. The energy conservation is obtained through a Neumann-type boundary condition which expresses that there is no enthalpy or entropy flux through the end-walls. Mixing losses can eventually be added through source terms in equation (2.2).

2.9 Experimental work

Besides theoretical developments, experimental data can be found. A classical test case is the Larguier Rotor (Larguier, 1980) tested at ONERA. Test data are available downstream of a rotor blade row, showing a radial flow profile which can be interpreted as a superposition of the different secondary flow contributions (Adkins and Smith, 1982). Dring et al. (1982) made extensive experiments at four stations downstream of a rotor blade row, at several radial positions, and at four different flow rates. Other wake data are available from the Pennsylvania State University (Ravindranath, 1980, Reynolds, 1979). Two three-stage compressors, differing primarily in aspect ratio, were designed and tested at Pratt & Whitney Aircraft under NASA sponsorship (Burdsall et al, 1979, Behlke et al, 1979). The effects of mixing are seen to be very strong for both configurations (see figure 1.1).

Less detailed data are available for the profile boundary layer radial flows. Recently, data were made available by Lakhsminarayana and Popovski (1987). Extensive data are presented at both pressure and suction side of a compressor rotor blade, at five radial positions and three axial stations.

3. APPROACH

Since convective mixing effects are to be considered, it is important to determine the different secondary flow of figure 2.1 with a reasonable accuracy. The strategy used to find the radial velocities is illustrated on figure 3.1. Five steps can be considered in the global flow computation :

(i) Through flow computation
(ii) Computation of the non-free vortex contribution
(iii) Computation of end-wall boundary layer secondary flows
(iv) Computation of profile boundary layers and wakes
(v) Radial redistributions including turbulent diffusion effects

The through flow computation delivers a flow which can be considered as the 'primary flow'. The secondary flow due to an eventual non-free vortex behaviour is next computed from passage averaged vorticity and continuity equations. The obtained velocities are superposed on the primary flow and therefore affect the subsequent steps. The end-wall boundary layer computation delivers a passage averaged cross flow component, confined to the end-wall regions. This cross flow includes the effects of end-wall viscosity, force defects and tip clearance flows (De Ruyck and Hirsch, 1981, 1982, 1983) and it generates an additional radial velocity component as a consequence of continuity. The obtained velocity components are superposed on the previous ones and affect the last step which is the computation of the 3D profile boundary layers and the 3D asymmetric wake. It is to be observed that all the secondary flows are determined in surfaces normal to the S1 and S2 surfaces, that is in surfaces of constant axial coordinate z (De Ruyck and Hirsch, 1981, 1982, 1983). Secondary vorticities are therefore written in terms of the axial vorticity component ω_z and secondary cross flows through an angular velocity component $w_{\theta.sec}$. A full computation of the transport equation which uses the secondary flow as input finally delivers the radial redistributions.

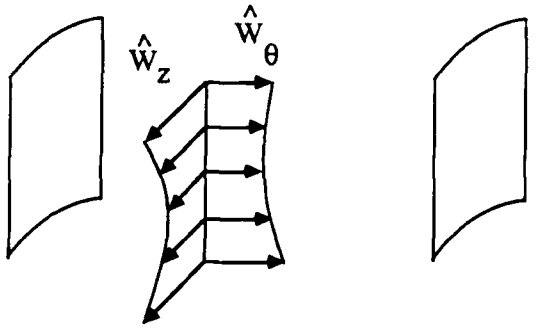

THROUGH FLOW COMPUTATION :

passage averaged velocities

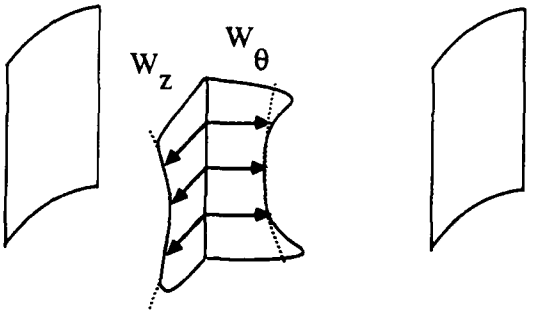

END-WALL BOUNDARY LAYER COMPUTATION :

passage averaged velocities including :
- EWBL viscous effects
- EWBL cross flows
- Tip clearance flows

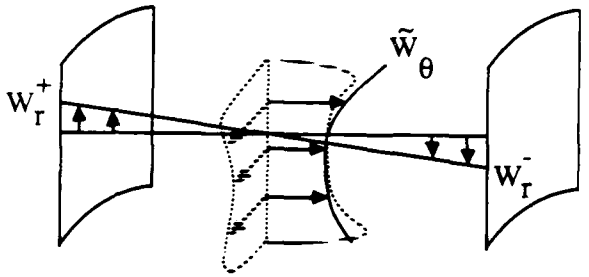

PASSAGE RADIAL FLOW COMPUTATION :

Passage radial flows including :
- All EWBL effects
- Main flow non-uniformity effects
- Circulation changes

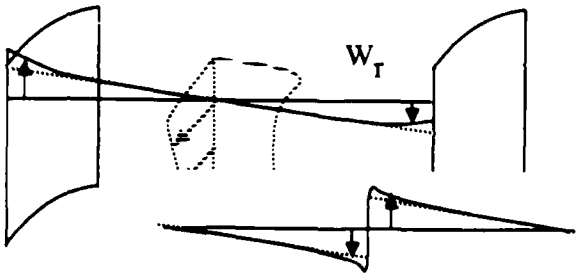

PROFILE BOUNDARY LAYER
AND WAKE COMPUTATION :

Detailed radial velocities including
profile boundary layer and wake radial flows

Figure 3.1 : Secondary flow computation strategy

4. THROUGH FLOW COMPUTATION

The background of the present work lies in the Quasi 3D approach presented in (Hirsch and Warzee, 1979). In this approach, correlations are used to compute the passage-averaged profile losses and deviations. Spanwise passage averaged profiles of all the primary flow properties are thus available.

5. RECONSTRUCTION OF SECONDARY FLOWS FROM PITCH AVERAGED VORTICITIES

Steps (ii) and (iii) will deliver passage averaged values of the axial vorticity $\tilde{\omega}_z$. This quantity is not sufficient for the reconstruction of the corresponding secondary flow velocities and additional information is to be supplied. This is done by a pitchwise modeling of the secondary flow components. A classical model for the secondary flow consists in a linear behaviour for the radial velocity $w_{r.sec}$ and a quadratic behaviour for the angular velocity $w_{\theta.sec}$ (Mellor and Wood, 1971):

$$
\begin{aligned}
w_{r.sec} &= \frac{1}{2} \times \Delta w_r \\
w_{\theta.sec} &= \frac{3}{2} \tilde{w}_{\theta.sec} \quad (1 - x^2) \qquad (5.1) \\
\text{where} \quad x &= \frac{2r}{s} (\theta - \theta_{\text{mid-pitch}})
\end{aligned}
$$

Δw_r is de difference in radial velocity between pressure and suction side of the passage (see figure 3.1). The secondary flow velocities can be determined from the knowledge of $\tilde{\Delta w}_r$ and $\tilde{w}_{\theta.sec}$, which are to be found from the knowledge of the vorticity $\tilde{\omega}_z$. The passage averaged vorticity is given by

$$
\tilde{\omega}_z = \frac{1}{r} \frac{\partial}{\partial r} \tilde{r w}_\theta - \frac{1}{s} \Delta w_r \qquad (5.2)
$$

where the passage averaged velocity $\tilde{w}_\theta$ can be decomposed as

$$
\tilde{w}_\theta = \hat{w}_\theta + \tilde{w}_{\theta.sec} \qquad (5.3)
$$

Equation (5.3) superposes the contributionss from the through flow computation (primary flow $\hat{w}_\theta$) and from the passage averaged secondary flow

($\tilde{w}_{\theta.sec}$). The incompressible secondary flow continuity equation in a surface normal to the axial velocity can be written as follows

$$\frac{1}{r}\frac{\partial}{\partial\theta} w_{\theta.sec} + \frac{\partial}{\partial r} w_r = 0 \tag{5.4}$$

The continuity equation (5.4) assumes that no secondary flow components are present in the axial direction, hence

$$\tilde{w}_z = \hat{w}_z \tag{5.5}$$

Taking the passage average of equation (5.4) with the secondary flow model of equation (5.1) yields

$$\frac{12}{s}\,\tilde{w}_{\theta.sec} = \frac{\partial}{\partial r}\Delta w_r \tag{5.6}$$

Using equation (5.3) for $\tilde{w}_\theta$ and equation (5.6) for $\tilde{w}_{\theta.sec}$ reduces equation (5.2) to

$$\frac{1}{12r}\frac{\partial}{\partial r}\left(rs\frac{\partial}{\partial r}\Delta w_r\right) - \frac{1}{s}\Delta w_r = \tilde{\omega}_z - \frac{1}{r}\frac{\partial}{\partial r} r\hat{w}_\theta \tag{5.7}$$

Equation (5.7) is a one dimensional second order equation for Δw_r with as boundary conditions a zero radial flow at hub and casing. It delivers the radial flows from the knowledge of $\tilde{\omega}_z$ and $\hat{w}_\theta$. It can easily be solved with a central difference scheme and inversion of a tridiagonal matrix. The only assumptions made consist in the pitchwise modelling of the secondary flow velocities described in equation (5.1). Application to a straight cascade (r>>) would reduce equation (5.7) to the following, in the case of a constant r.h.s.

$$\Delta w_r = s\left(\frac{\partial \hat{w}_\theta}{\partial r} - \tilde{\omega}_z\right)\left(1 - \frac{e^{ay} + e^{-ay}}{e^{ah} + e^{-ah}}\right) \tag{5.8}$$

where

$$\begin{aligned} a &= 2\sqrt{3}/s \\ h &= \text{half span} \\ y &= r - r_{\text{mid-span}} \end{aligned} \tag{5.9}$$

Equation (5.8) is a simple result which can be used in the case of constant

r.h.s. in equation (5.7).

In the present approach two distinct contributions to ω_z are searched, and superposed

$$\tilde{\omega}_z = \tilde{\omega}_{z.inv} + \tilde{\omega}_{z.ewbl} \tag{5.10}$$

$\tilde{\omega}_{z.inv}$ is the secondary vorticity due to an eventual non-free vortex behaviour of the main flow, $\tilde{\omega}_{z.ewbl}$ is the secondary vorticity due to the end-wall boundary layer flows. This last contribution is zero outside of the end-wall regions. Both contributions are discussed below.

6. SECONDARY FLOWS FROM NON-FREE VORTEX BEHAVIOUR

The radial flows inside the passage are found from the incompressible inviscid vorticity equation

$$(\vec{W}.\vec{\nabla}).\vec{\omega} - (\vec{\omega}.\vec{\nabla}).\vec{W} = 0 \tag{6.1}$$

Since the secondary flow is searched in surfaces z=cte, only the axial component of the secondary vorticity is relevant. The idea of the present approach is to passage average the axial component of equation (6.1) which yields the following relation (see appendix B)

$$\begin{aligned} \tilde{w}_z \frac{\partial}{\partial z} \tilde{\omega}_z \Big|_{inv} = {} & \tilde{\omega}_z \frac{\partial}{\partial z} \tilde{w}_z + (\tilde{\omega}_\theta - tg\beta\, \tilde{\omega}_z) \frac{1}{s} \Delta w_z \\ & - (\tilde{w}_\theta - tg\beta\, \tilde{w}_z) \frac{1}{rs} \frac{\partial}{\partial r} (r \Delta w_z tg\beta) \Big|_{inv} \end{aligned} \tag{6.2}$$

Equation (6.2) is to be written in the absolute reference system. β is the blade angle, Δ indicates the difference (suction side - pressure side) for a rotor and the inverse for a stator. The subscript 'inv' indicates that the end-wall boundary layers are not considered in this equation. The only approach made is the neglection of second order pitchwise fluctuation terms. The averaged vorticities are given by

$$\begin{aligned} \tilde{\omega}_{z.inv} &= \frac{1}{r} \frac{\partial}{\partial r} r\tilde{w}_\theta - \frac{1}{s} \Delta w_r \Big|_{inv} \\ \tilde{\omega}_{\theta.inv} &= \frac{\partial}{\partial z} \tilde{w}_r - \frac{tg\beta}{s} \Delta w_r - \frac{\partial}{\partial r} \tilde{w}_z \Big|_{inv} \end{aligned} \tag{6.3}$$

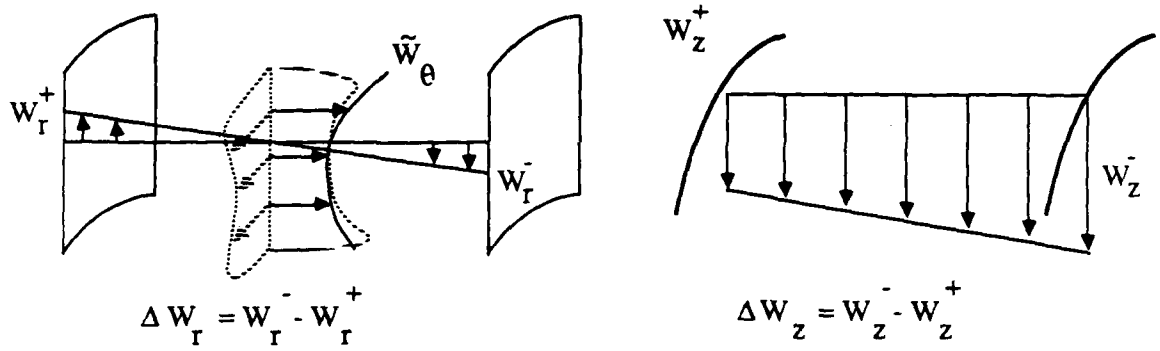

Figure 6.1 : Passage radial flow computation

Δw_z represents the difference in axial velocity between suction and pressure side of a rotor blade (or the inverse in a stator blade, see figure 6.1). This difference is a consequence of zero vorticity in the radial direction

$$\omega_r = \frac{1}{r}\frac{\partial w_z}{\partial \theta} - \frac{1}{r}\frac{\partial r w_\theta}{\partial z} = 0 \qquad (6.4)$$

which yields after passage averaging

$$\frac{1}{s}\Delta w_z = \cos^2\beta \frac{1}{r}\frac{\partial}{\partial z}(r\bar{w}_{\theta.inv}) \qquad (6.5)$$

As a consequence of equation (5.15), the last contribution in equation (5.12) results from changes in angular momentum along the blades.

After substitution of equations (6.3) and (6.5) in equation (6.2), three unknowns subsist : $\bar{\omega}_{z.inv}$, $\Delta w_{r.inv}$ and $\bar{w}_{\theta.inv}$. $\bar{w}_{\theta.inv}$ can be expressed as a fuction of $\Delta w_{r.inv}$ by substituting equation (5.6) in equation (5.3). The remaining two unknowns will be found by solving equations (5.7) and (6.2) simultanuously, after inclusion of the end-wall boundary layer contributions through equation (5.10).

7. END-WALL BOUNDARY LAYERS

End-wall boundary layers (EWBL) are predicted through a 3D integral method where end-wall secondary flows and clearance effects are introduced (De Ruyck and Hirsch, 1981, 1982, 1983). The method originates from Mellor and Wood's approach (1971) where rigorous integral boundary layer equations were written for the end-wall boundary layers, including force defect

thicknesses. In this work, simplified assumptions such as constant shape factor or skin friction were made and the equations were integrated from inlet to outlet of a blade row. This approach was extended by De Ruyck and Hirsch (1981) to include velocity profile models and correlations for secondary flow and tip clearance effects through the defect forces. It is assumed that all the secondary and tip clearance effects originate inside the EWBL and the additional losses are taken into account separately when computing the overall efficiency (De Ruyck and Hirsch, 1981, 1982, 1983).

The EWBL method is summarised in appendix C, it essentially solves an equation of the type

$$\frac{1}{r}\frac{d}{dz}\rho r \hat{w}_z^2 \vec{\theta}_z + \rho \hat{w}_z \frac{d}{dz}\hat{\vec{W}} = \vec{\tau} + \vec{F} \tag{7.1}$$

where

$$\begin{aligned} \hat{w}_z^2 \vec{\theta}_z &= \int_o^\delta (\hat{\vec{W}} - \vec{W})\, w_z dr \\ \hat{w}_z \delta_z^* &= \int_o^\delta (\hat{w}_z - w_z)\, dr \end{aligned} \tag{7.2}$$

The velocities indicated with a carat ^ are obtained from the through-flow computations. Extra relations are obtained with Head's entrainment equation, Ludwig Tillman's skin friction relation and correlations for the defect force $\vec{F}$. Closure is obtained by the use of the following passage averaged velocity profile models

$$\frac{\bar{w}_{z.ewbl}}{\hat{w}_z} = 1 - b\left(1 - \frac{y}{\delta}\right)^n \tag{7.3}$$

$$\frac{\bar{w}_{\theta.ewbl}}{\hat{w}_z} = (1-b)\,tg\varepsilon'_w \left(1 - \frac{y}{\delta}\right)^n \tag{7.4}$$

The cross-flow components of the end-wall boundary layer generate radial flows which can be found from equation (5.7), through the contribution $\bar{\omega}_{z.ewbl}$. The vorticity associated with the boundary layer is assumed to be

$$\bar{\omega}_{z.ewbl} = \frac{1}{r}\frac{\partial}{\partial r} r \bar{w}_{\theta.ewbl} \tag{7.5}$$

It is added to the vorticity $\bar{\omega}_{z.inv}$ which is found from equation (6.2). The simultaneous solution of equations (5.7), (5.10), (6.2) and (7.5) delivers values for $\Delta w_{r.sec}$ and $\bar{w}_{\theta.sec}$ which contain the secondary flows resulting from non-free vortex and end-wall boundary layer effects.

8. PROFILE BOUNDARY LAYER RADIAL FLOWS

Boundary layers along turbomachine blades are three dimensional and contribute to both the radial convection and turbulent diffusion. Experimental and theoretical information about these radial flows is poor. Adkins and Smith (1982) estimate these radial flows by solving the local conservation of radial momentum along the blade, introducing two empirical constants. The radial velocity is found to be a direct consequence of the boundary layer velocity gradient. Whitfield and Keith (1985) used the same base but included the blade loading effects by means of the loss correlations of Koch and Smith (1976).

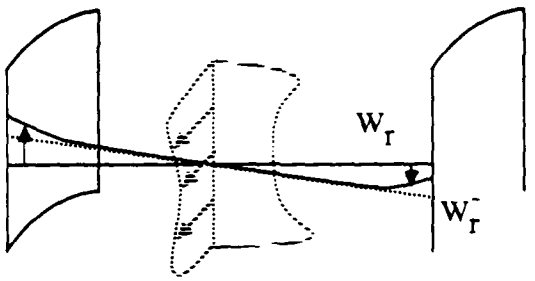

Figure 8.1 : radial flows from profile boundary layers

In the present approach, the boundary layer equations are developed in the cilindrical coordinate system, and not in a coordinate system associated to the profile walls, which is a rather unusual way to proceed. It presents however some practical advantages such as an easier theoretical development and an easier computation. The 3D integral boundary layer equations used can be found in appendix D. Velocity profiles are introduced in order to obtain closure. In analogy with the EWBL profile models, following model equations are introduced

$$\frac{w_s}{w_s} = 1 - b\left(1 - \frac{y}{\delta}\right)^n \qquad (8.1)$$

$$\frac{w_r - w_s tg\alpha_r}{w_s} = (1-b)tg\varepsilon'_w \left(1 - \frac{y}{\delta}\right)^n \qquad (8.2)$$

where s lines are the projection of streamlines on an axisymmetric stream surface. α_r is the radial flow angle. The parameters b and n are correlated through the following relation (De Ruyck and Hirsch, 1981, 1983)

$$b = e^{-10n\sqrt{C_f}} \qquad (8.3)$$

9. WAKE FLOW

The wake can be considered as an important element in the total radial flow analysis. Peak values in radial velocity are observed in the near wake, where very low velocities may induce a high centrifugation. Adkins and Smith (1982) and Whitfield and Keith (1985) treated the wake by writing the mainstream and radial momentum conservation laws along the wake center. They characterise the radial flows by 'peak' radial velocities at the wake center whereas the total amount of radial flow is found by modeling the wake profiles. Since symmetric wake models are used, they are not able to simulate asymmetric radial wake profiles.

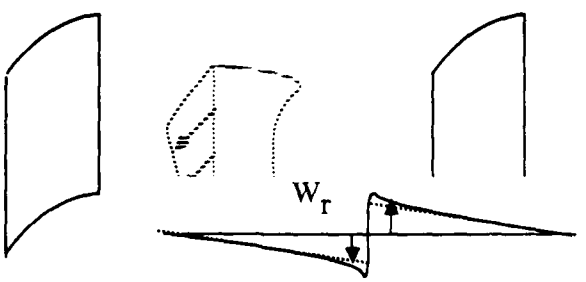

Figure 9.1 : wake radial flows

In the present wake approach, pressure and suction side of the wake are

treated separately and the concept of 'peak velocities' is not used. The reason for this is that wake profiles may be very asymmetric, and pressure and suction side radial flows may even have opposite signs as appears in the experiments of Dring et al. (1982).

9.1 Wake profiles

A model is introduced determined by a function f and the skewing angle ε. It is valid at one of the wake sides, the two wake sides being coupled via a 'bridge' function g

$$\frac{w_s}{w_s} = 1 - bf(\eta) - (\bar{b}-b)\, g(\eta) \tag{9.1}$$

$$\begin{aligned}\frac{w_r - w_s \mathrm{tg}\alpha_r}{w_s} &= (1-b)\mathrm{tg}\varepsilon\, f(\eta) \\ &+ \left[(1-\bar{b})\mathrm{tg}\bar{\varepsilon} - (1-b)\mathrm{tg}\varepsilon\right] g(\eta) \\ &+ (1-\bar{b})(\mathrm{tg}\bar{\alpha} - \mathrm{tg}\alpha)\, g(\eta)\end{aligned} \tag{9.2}$$

where

$$\eta = \frac{y}{\delta}$$

$$f(\eta) = 1 - 6\eta^2 + 8\eta^3 - 3\eta^4 \tag{9.3}$$

$$g(\eta) = e^{-\eta/\eta_0} \tag{9.4}$$

The angle α_r is the radial flow angle. It may differ from pressure side to suction side and depends directly on Δw_r. The overbars indicate mean values between pressure (+) and suction (-) side such as

$$\bar{b} = \frac{b^+ + b^-}{2} \tag{9.5}$$

The function f approaches the classical probability function (Korkan et al., 1977) used to model wake profiles. The function g corrects the profile in the neighbourhood of the centerwake to fit with the opposite wake side. It affects the profile over a distance determined by η_0. At η=0, the velocities reduce to (for both sides)

$$\frac{w_s}{w_s} = 1 - \bar{b} \tag{9.6}$$

$$\frac{w_r}{w_s} = (1-\bar{b})\left(tg\bar{\varepsilon} + tg\bar{\alpha}\right) \tag{9.7}$$

For small values of η_o, pressure and suction side of the wake conserve their identity, at higher values both sides are mixed and the wake shape becomes more symmetric (figure 9.2). High second derivatives are present around the centerline and the asymmetry gives rise to a diffuse mixing between pressure and suction side of the wake. Hence η_o can be approached by

$$\eta_o = \frac{1}{\delta}\sqrt{\varepsilon_t \Delta z / w_z} \tag{9.8}$$

where Δz is the distance from the trailing edge and ε_t is the eddy viscosity which will be discussed below.

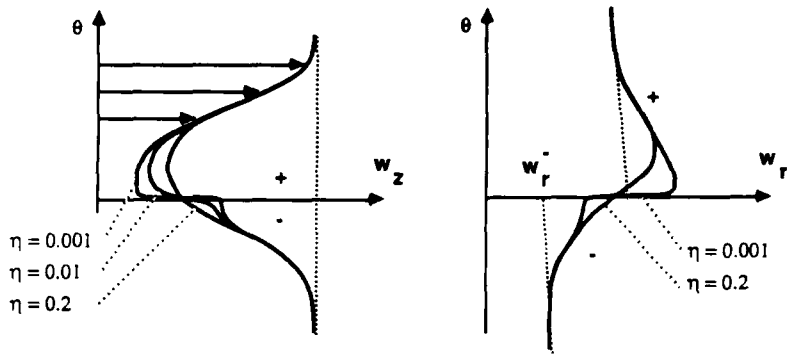

Figure 9.2 : Asymmetric wake profile model

9.2 Wake momentum equations

Three-dimensional integral wake momentum equations are used (appendix D). Since pressure and suction side of the wake are considered separately, two sets of integral equations can be considered. In practice, numerical instability was however observed when using the radial momentum equation separately at pressure and suction side, and only one equation integrated over the whole wake is retained. This radial momentum equation mainly controls the mean skewing $tg\bar{\varepsilon}$. As long as the wake is asymmetric a mid-wake

friction term is present in the axial momentum equation. It is given by

$$\tau_s^+ = -\tau_s^- = \varepsilon_t \frac{\hat{w}_s}{\delta'} \frac{1}{2\eta_0}(b^- - b^+) \tag{9.9}$$

As a consequence, the friction tends to decrease the difference between momentum thicknesses at pressure and suction side.

9.3 Local wake decay equations

Expressing the integral momentum equations yields three equations for 6 unknowns :

δ^+, δ^- : pressure and suction side wake thickness
b^+, b^- : pressure and suction side wake velocity defect
ε^+, ε^- : pressure and suction side skewing angle

In order to obtain closure, three extra relations are needed which are found by expressing the conservation of momentum at the wake center. The classical meridional momentum equation at wake center is found to be (see appendix E)

$$\frac{1}{\bar{b}} \frac{\partial \bar{b}}{\partial z} = -\frac{12\varepsilon_t}{(1-\bar{b})\bar{\delta}^2 w_z} - \frac{(2-\bar{b})}{(1-\bar{b})} \frac{1}{\hat{w}_z} \frac{\partial \hat{w}_z}{\partial z} \tag{9.10}$$

Equation (9.10) directly controls the center wake velocity defect $\bar{b}$. The next relations seek for more information about the differences $\Delta b = b^+ - b^-$ and $\Delta tg\varepsilon = tg\varepsilon^+ - tg\varepsilon^-$. This is obtained by writing the momentum equations in two points close to the wake center, but far enough from each other such that these points are not affected by the opposite wake side. The subtraction of the two obtained relations yields information about the differences between pressure and suction side. This can be done by expressing the momentum equations in a point η_1, where η_1 is such that

$$1 = f_1 >> g_1 \tag{9.11}$$

Doing this at both wake sides and subtracting yields, after some manipulation (see appendix E)

$$\frac{1}{\Delta b}\frac{\partial \Delta b}{\partial z} = -\frac{12\varepsilon_t}{\delta^2 w_z(1-b)} + \frac{1}{(1-b)}\frac{\partial \bar{b}}{\partial z} - \frac{2}{w_z}\frac{\partial \hat{w}_z}{\partial z} \tag{9.12}$$

$$\frac{1}{\Delta(tg\alpha+tg\varepsilon)}\frac{\partial}{\partial z}\Delta(tg\alpha+tg\varepsilon) = -\frac{12\varepsilon_t}{\delta^2 w_s(1-b)} - \frac{1}{w_s}\frac{\partial \hat{w}_s}{\partial z} \tag{9.13}$$

The radial velocities obtained from equations (9.1) and (9.2) are added to the secondary velocities $w_{r.sec}$ and $w_{\theta.sec}$.

10. MIXING EQUATION

The superposition of the different secondary flow contributions is used in the radial mixing equations. The solution for the radial redistributions of e.g. the temperature T is to be found from the steady state transport equation

$$(\vec{w}.\vec{\nabla})\ T = \varepsilon_t \Delta T \tag{10.1}$$

where the convective velocity is reduced to the secondary flow velocity, which gives (neglecting curvature)

$$w_z\frac{\partial T}{\partial z} = -w_{\theta.sec}\frac{1}{r}\frac{\partial T}{\partial \theta} - w_{r.sec}\frac{\partial T}{\partial r} + \varepsilon\left(\frac{1}{r}\frac{\partial}{\partial r}r\frac{\partial T}{\partial r} + \frac{1}{r^2}\frac{\partial^2 T}{\partial \theta^2}\right) \tag{10.2}$$

In fact, it is possible to use equation (10.2) in this shape and to solve it numerically by using a two-dimensional upwind discretisation. This procedure is not expensive and makes use of the complete available secondary flow field. The mixing equation of Adkins and Smith (1982) results in the following passage averaged equation

$$\tilde{w}_z\frac{\partial \tilde{T}}{\partial z} = \varepsilon_c\frac{\partial^2 \tilde{T}}{\partial r^2} \tag{10.3}$$

where the convective mixing coefficient is given by

$$\varepsilon_c = \frac{z}{s}\int_{pitch}\left(\frac{w^2_{r.sec}}{w^2_z}\right)dx \tag{10.4}$$

The mixing equation proposed by Adkins and Smith is a simpler alternative, which however is not able to simulate all the convective effects, as will be shown in the following results.

In practice mixing is to be performed on the total temperature (Hirsch and Dring, 1987). In the present report it will be considered that $V^2/2cp << T$ and the mixing is considered on the static temperature T.

11. TURBULENT MIXING COEFFICIENT

A turbulent mixing coefficient appears in the wake equations (9.8) to (9.12), and in the mixing equation (10.2). According to Schlichting (1955), following expression can be used in the wake

$$\varepsilon_t = K\delta b \hat{w}_z \qquad (11.1)$$

where δ denotes the physical wake thickness, K depends on the turbulence intensity. Following values were observed when applying the wake theory on some test cases (De Ruyck and Hirsch, 1987)

K = 0.005 for an airfoil wake with thin trailing edge
K = 0.010 for a compressor blade wake at design point
K = 0.045 for a compressor blade wake near stall
K = 0.047 for a cylinder wake (Schlichting, 1955)

leading to (UTRC compressor, Dring et al., 1982)

$$\frac{\varepsilon_t}{w_z L} = 0.001 \text{ for a compressor blade wake at design point}$$

$$\frac{\varepsilon_t}{w_z L} = 0.006 \text{ for a compressor blade wake near stall}$$

These values are of the same order as the global mixing coefficients observed by Gallimore and Cumpsty (1986). It is interesting to compare these values with the relation proposed in (Gallimore and Cumpsty, 1986) :

$$\frac{\varepsilon_t}{w_z L} = A \frac{t}{L} \left[\frac{2\bar{\omega}(t/L)}{3\phi^2} \right]^{1/3} \qquad (11.2)$$

where $A = \left[\frac{\overline{u'v'}}{q^2} \right]^{1/2}$, t is the airfoil thickness, $\bar{\omega}$ the loss coefficient, ϕ the flow coefficient and L the axial stage length. The above values of 0.001 and 0.006 are obtained when taking for A, in the particular case of the UTRC rotor (Dring et al., 1982) and when estimating the loss coefficient from the wake momentum thickness,

A ≈ 0.1 for a compressor blade wake at design point
A ≈ 0.3 for a compressor blade wake near stall

The value A ≈ 0.4 proposed in (Gallimore and Cumpsty, 1986) corresponds to quite high values of the Reynolds stress and the present values are in better agreement with current data. A good coherence is thus found between the wake diffusivity and both the experimental and theoretical values of Gallimore and Cumpsty (1986). As a consequence it is not unreasonable to consider the wake mixing coefficient as representative for the overall mixing coefficient, and the assumption can be made that the level of turbulent diffusion in the radial mixing process is equal to the level found in the wake decay. In this case, the sole free (empirical) parameter of the present model is the turbulent diffusion coefficient ε_t.

12. RESULTS

Three test cases are considered in the present report

i) A linear compressor cascade tested at the Dept. of Fluid Mechanics at the Vrije Universiteit Brussel

ii) An Onera compressor rotor investigated by Larguier (1980)

iii) An UTRC compressor rotor by Dring et al. (1982)

These three cases have very different secondary flows, and consequently a different radial mixing behaviour. The cascade has no centrifugation effects. The blades of the Larguier rotor have a radially constant solidity and no twist, giving rise to a a substantial non-free vortex behaviour. The UTRC rotor is more representative for industrial machines, where all the discussed effects are present.

The following results show secondary flow fields, corresponding passage averaged temperature profiles, temperature contour plots and contour plots of a tracer gas injected at the leading edge. The location of the tracer gas injection point is indicated by a black spot. Four lines are drawn on the passage averaged temperature results (e.g. figure 12.2.b). The dotted line is an arbitrary input temperature (or other) profile which is either quadratic or linear (constant second derivative or zero second derivative). The dashed line is obtained from a one dimensional diffusion process through

$$\tilde{w}_z \frac{\partial \tilde{T}}{\partial z} = \varepsilon_t \frac{\partial^2 \tilde{T}}{\partial r^2} \qquad (12.1)$$

This equation is one dimensional and solved with as boundary conditions $\frac{\partial T}{\partial r} = 0$ at the end-walls (adiabatic machine). The solid lines with triangles are obtained from the same equation, but with ε_t replaced by

$$\varepsilon = (z-z_o)\ \tilde{w}_z \int_{pitch} \left(\frac{w_r^2}{w_z^2} \right) r\, d\theta + \varepsilon_t \qquad (12.2)$$

This is the coefficient of Adkins and Smith (1982) (without the additional corrections) plus turbulent diffusion. The value z_o was taken at leading edge, the radial velocities being local values. The solid line with squares is obtained from the computation of equation (10.2). This equation is

solved through a two-dimensional upwind discretisation. The results on the figures are passage averaged values of the resulting temperature fields.

	Linear Cascade	ONERA rotor	UTRC rotor
Aspect ratio	1	0.89	1
Solidity	1.11	1.34	1
hub/tip radius	-	0.68	0.8
Blade inlet angle	33°	50°	59.5°
Blade outlet angle	-13°	30°	17.5°
Flow coefficient	-	0.74	0.75
Absolute deflection	34°	30°	33°

Table 1 : Blade geometries at mid-span

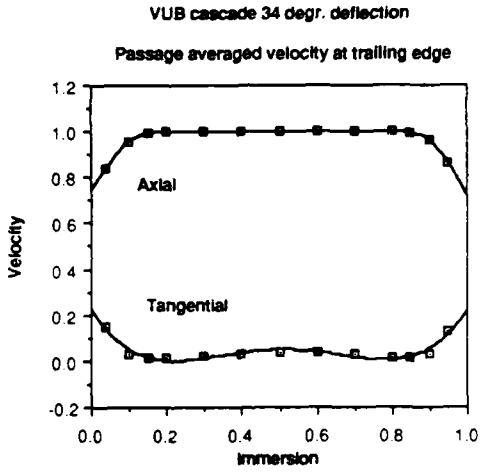

Figure 12.1 : Passage averaged cross flow in a linear cascade at the trailing edge
solid line : computation
squares : experiment

12.1 LINEAR CASCADE

The geometry of the cascade is summarized in table 1. Experimental 3D velocity fields are available in different planes upstream, inside and

downstream of the cascade. Detailed experimental data obtained in this cascade will be published elsewhere. Results are shown on figures 12.1 to 12.4. Figure 12.1 shows the experimental and the computed passage averaged velocities at the trailing edge. Figure 12.2 shows the computed secondary flow pattern for an overall deflection of 34° and the corresponding mixing results at 6 chords downstream of the trailing edge, the mixing effects at the trailing edge (not shown) being less relevant. The turbulent mixing coefficient has been taken as $\varepsilon_t/w_z L = 0.002$. The maximum radial flows reach about 3 % of the meridional velocity, but are zero at mid-span. In this particular case, the turbulent diffusion appears to be the dominating effect. The contribution from the radial convection can be seen from the the small differences between the dashed and the solid lines. An injected gas migrates slowly in the pitchwise direction, but the contour plot shows a dominating isotropic character.

In order to enhance the convection effects, the deflection has been arbitrarily increased to 54°, increasing the boundary layer overturning. The maximum radial velocity reaches 6% of the meridional velocity. The results are shown on figures 12.3 and 12.4. Convection effects become more important, and a clear difference appears between pure diffusion, the Adkins and Smith model and the present computation. The present computation on figure 12.3 shows that the high temperature at the end-wall is convected towards the mid-span and vice-versa, which is impossible to reproduce with a pure diffusion process. The contour plots of injected gas concentrations do not remain isotropic and indicate more important flow migrations. A linear inlet temperature (figure 12.4) increases the relative importance of the convection because of the zero second temperature derivatives at inlet. Figure 12.4.b shows the resulting temperature distributions at 6 chords downstream of the cascade.

12.2 ONERA ROTOR (Larguier, 1980)

The ONERA rotor has a non-free vortex design which generates an important secondary flow. Its geometry is summarised in table 1. The available data allow a validation of the wake prediction models as described by equations (9.1) and (9.2), as shown on figure 12.5 where the wake meridional and radial velocity profiles are drawn at 30% chord downstream of the trailing edge. The radial mixing results are shown at the trailing edge (figure 12.6) and at 1.5 chord distance downstream (figures 12.7 and 12.8). The

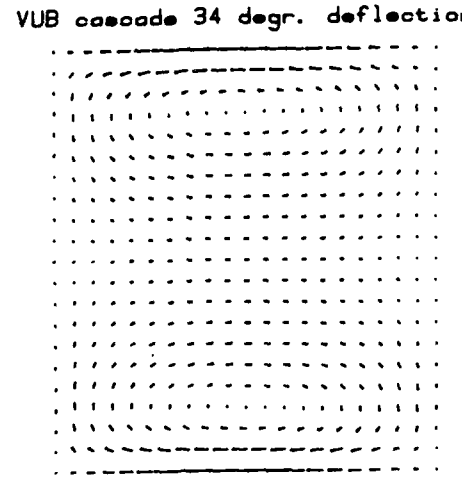

(a)

Secondary velocity field

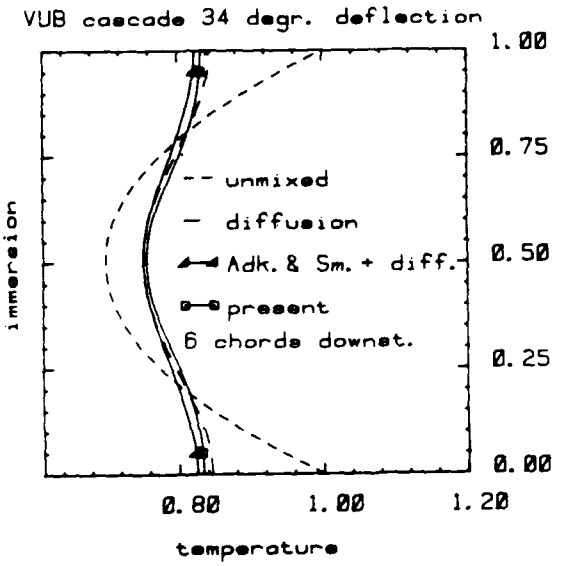

(b)

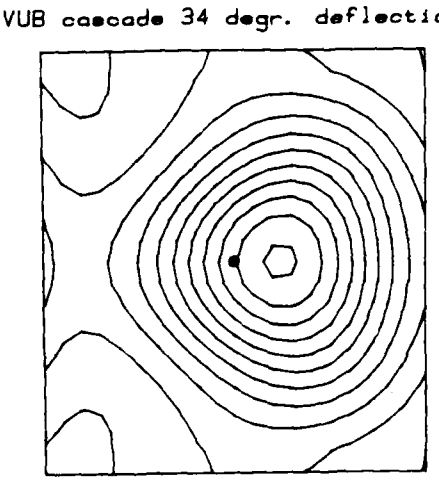

(c)

Gas concentration contour plot

Figure 12.2 : Secondary flow field and radial redistributions, linear cascade 34° deflection

turbulent mixing coefficient $\varepsilon_t/w_z L$ is about 0.002. The radial redistributions at the trailing edge are not very important and are again dominated by turbulent mixing, despite the high radial velocities which reach 20% of the main flow. At 1.5 chord distance results are found where the convection dominates. It is intresting to observe the similarity between the results from the Adkins and Smith approach and our computation, in the case of a quadratic inlet temperature (figure 12.7). In this particular case the radial velocities are such that the convection can be simulated by the diffusion process proposed by Adkins and Smith. Taking a linear temperature makes however the convection the dominating effect (figure 12.8).

12.3 UTRC ROTOR (Dring et al., 1982)

Results obtained with the UTRC rotor are shown on figures 12.9 to 12.12. The geometry of the rotor is summarized in table 1. Detailed velocity field measurements are available at four downstream stations. Measurements were made at four different flow coefficients (0.65, 0.75, 0.85 and 0.95).

Wake predictions

The results shown on figures 12.9 and 12.10 are taken from (De Ruyck and Hirsch, 1987) and were used to validate the wake theory. The data at the first experimental station were taken as input to start the wake computation. A correct behaviour of the wake theory is observed on both results. The lowest flow rate (figure 12.8) is close to the stall limit, whereas the higher one gives a certain amount of secondary flow due to a non-free vortex behaviour. Good agreement is in general observed. The values for K in equation (11.1) were found to be K=0.008 for the flow coefficient of 0.85 and K=0.045 for the flow coefficient of 0.65. The value for the dispersion coefficient increased considerably for the test case close to the stall limit, which can be explained by an important increase in turbulence. The corresponding values for $\varepsilon_t/w_z L$ are about 0.001 for the high and 0.006 for the lower flow rate. A strong radial flow is observed experimentally inside the wake close to the stall limit. Such a strong radial flow is not found when applying the profile boundary layer equations. It is probably due to separations in the neighbourhood of the trailing edge, causing a stronger wake centrifugation at this place, as stated by Dring et al. (1982).

Radial mixing prediction

Figure 12.11 shows the redistribitions at a flow coefficient of 0.75. The flow is overturned at the hub and somewhat underturned at the tip, where a clearance is present. The overall radial velocity level reaches only 2 to 3% of the meridional component, which is comparable with the 34° deflection cascade case. The peak wake radial velocities reach 7 to 8% of the meridional velocity. The turbulent mixing coefficient $\varepsilon_t/w_z L$ is about 0.002. The radial redistributions at 1 chord distance downstream of the trailing edge are not very significant and are dominated by turbulent diffusion. This result is again comparable with the cascade result which has a similar blade loading. The radial flows in the wake are high, but the total amount of fluid which is redistributed is not large enough to enhance the radial convection effects. Gas injections are simulated in the hub and casing end-wall boundary layers, and pitchwise flow migrations can be observed on figure 12.11. These migrations do not affect the passage averaged concentration (or temperature) profiles in a significant way, however.

Non isotropic diffusion

The experiments by Wisler et al. (1987) indicate that the flow redistributions may have a non-isotropic diffusive character. From the experimental contour plots on figure 12.12 it can be seen how diffusion is increased in the end-wall and profile boundary layer flows. A similar plot was computed in the UTRC rotor by taking

$$\frac{\varepsilon_t}{w_z L} = 0.001 \text{ in the main flow}$$

$$\frac{\varepsilon_t}{w_z L} = 0.008 \text{ in the boundary layers and wake} \qquad (44)$$

This ratio of the turbulent diffusion coefficient is required to obtain a qualitative agreement between the experimental and the computed contour plots, which indicates that a constant overall mixing coefficient is a limitative assumption. It also indicates that the overall radial redistributions may be dominated by the high turbulent diffusion in the wake.

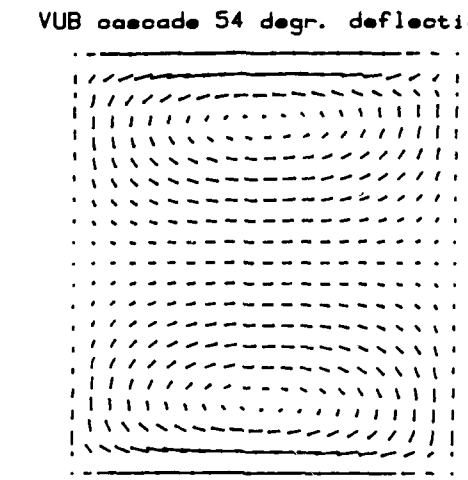

(a)

Secondary velocity field

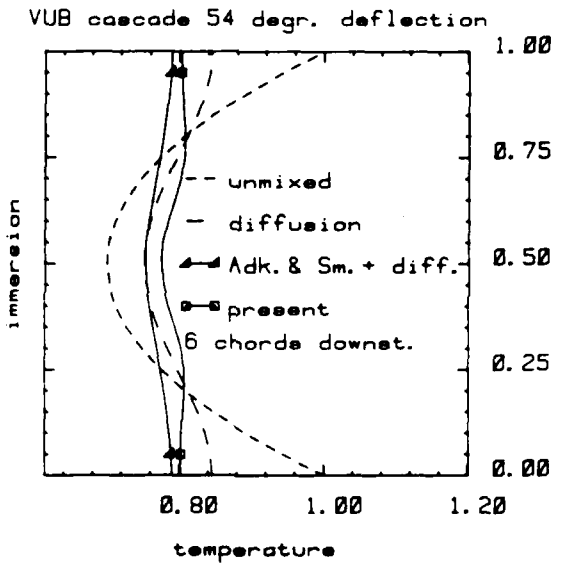

(b)

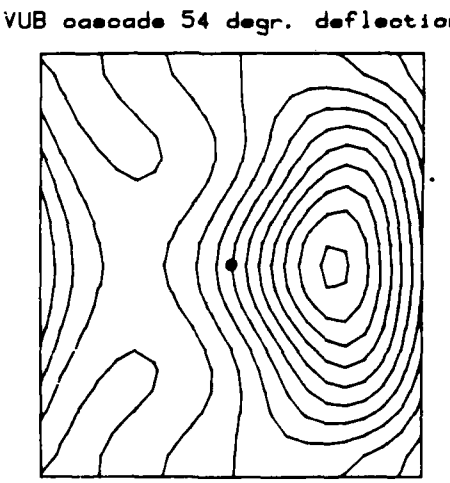

(c)

Gas concentration contour plot

Figure 12.3 : Secondary flow field and radial redistributions, linear cascade 54° deflection quadratic inlet temperature profile

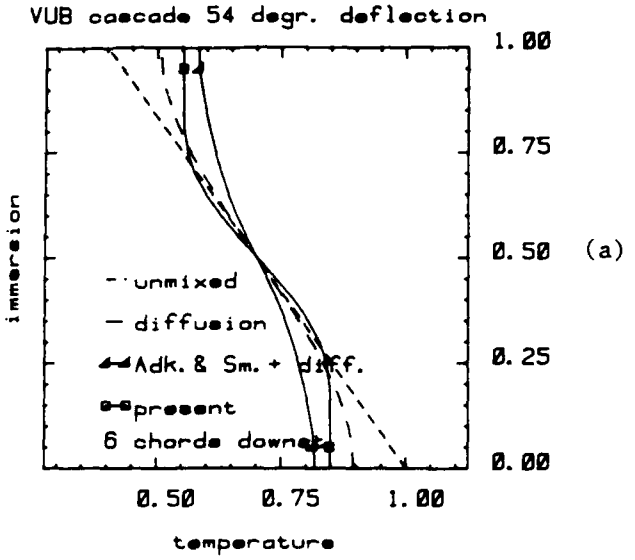

(a)

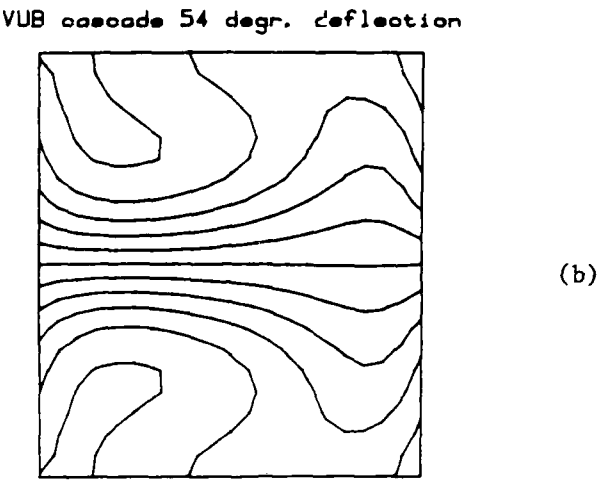

(b)

Figure 12.4 : Secondary flow field and radial redistributions, linear cascade 54° deflection linear inlet temperature profile

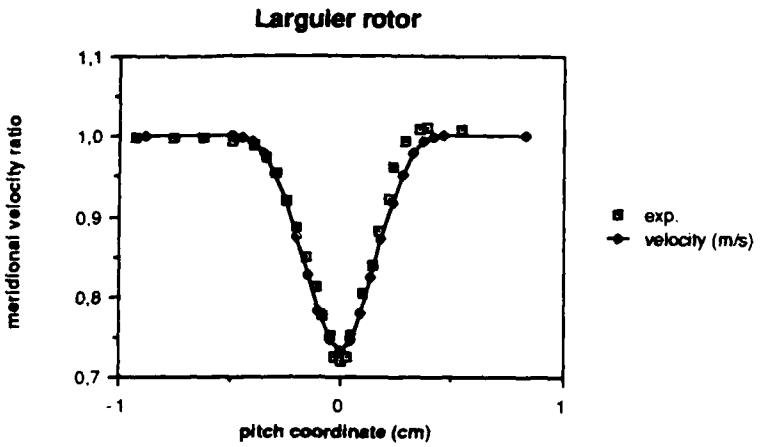

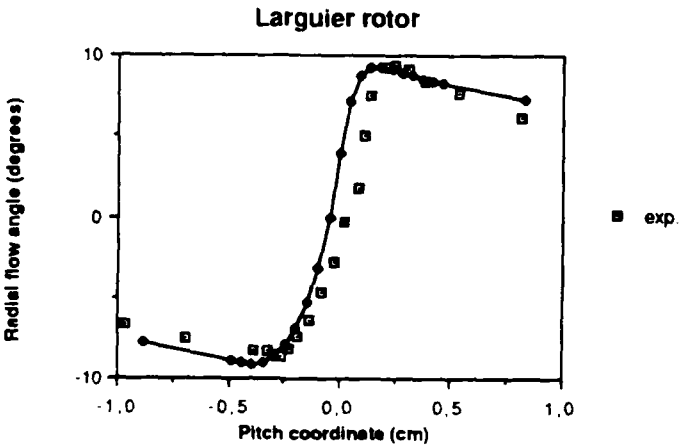

Figure 12.5 : Mid span meridional and radial flow in the Onera rotor at 30% chord distance downstream of the trailing edge
solid line : computation
squares : experiment (Larguier, 1980)

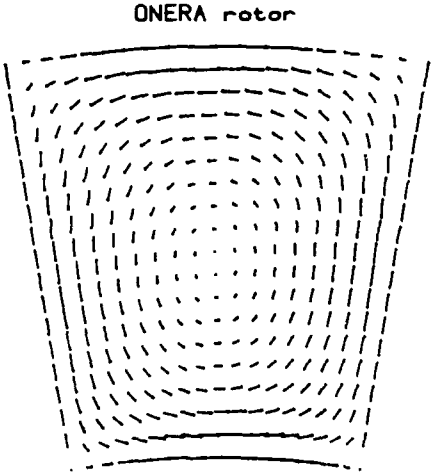

(a)

Secondary velocity field

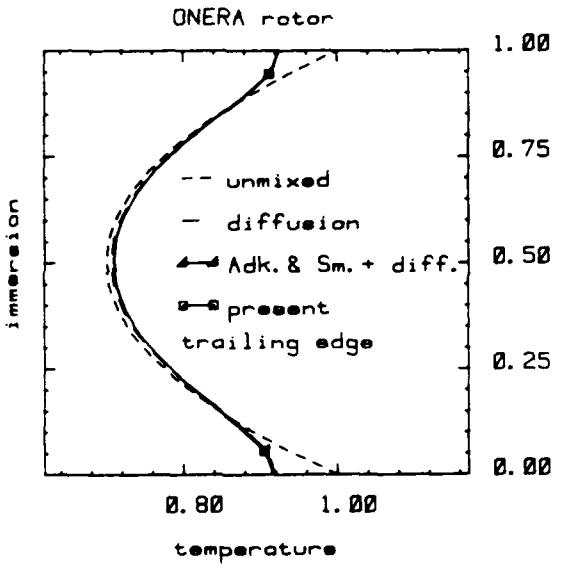

(b)

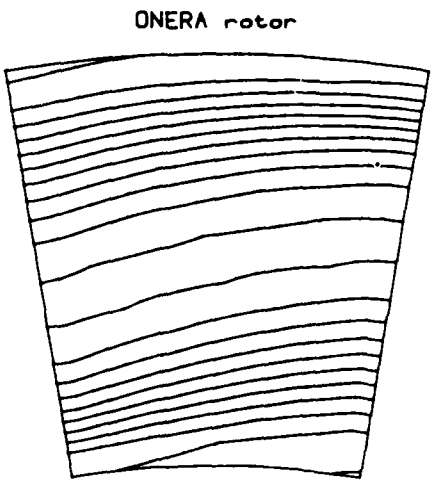

(c)

Temperature contour plot

Figure 12.6 : Secondary flow field and radial redistributions, Onera rotor at trailing edge

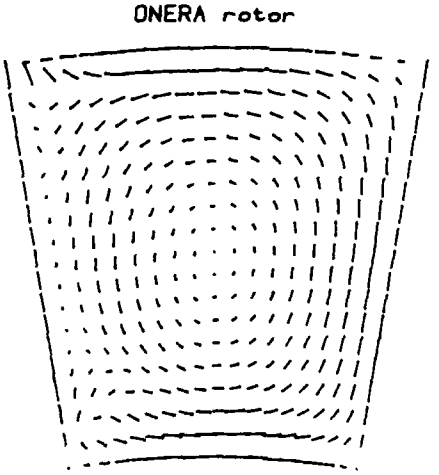

(a)

Secondary velocity field

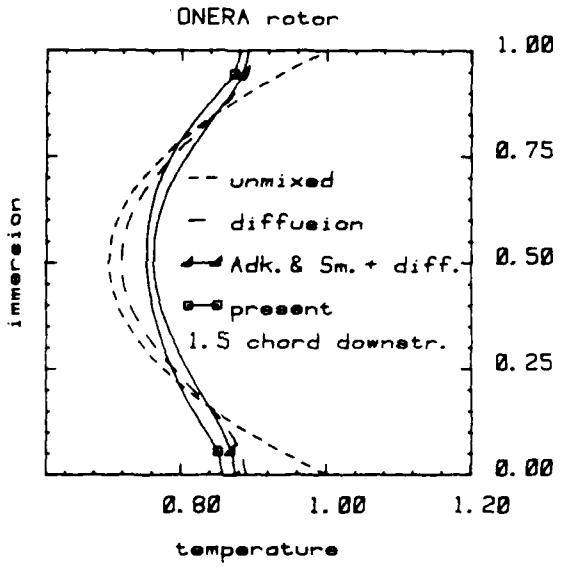

(b)

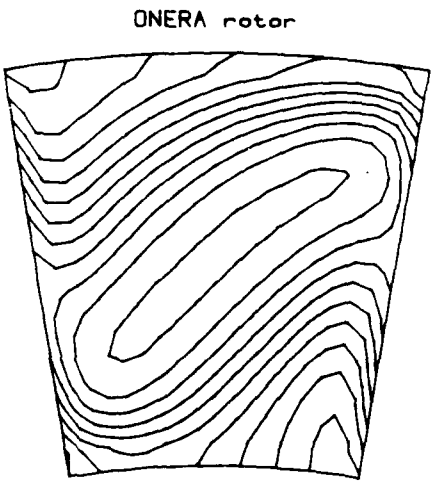

(c)

Temperature contour plot

Figure 12.7 : Secondary flow field and radial redistributions, Onera rotor, 1.5 chord distance downstream of the trailing edge quadratic inlet temperature profile

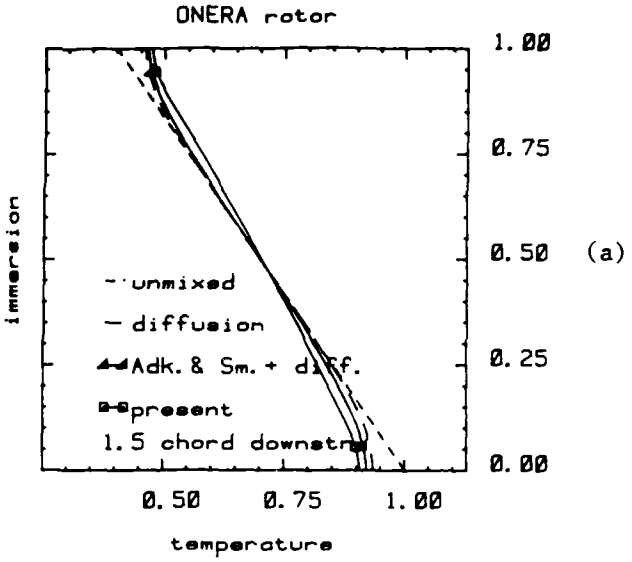

(a)

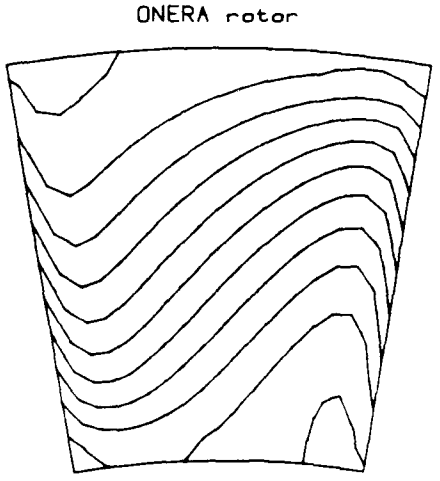

(b)

Temperature contour plot

Figure 12.8 : Secondary flow field and radial redistributions, Onera rotor, 1.5 chord distance downstream of the trailing edge linear inlet temperature profile

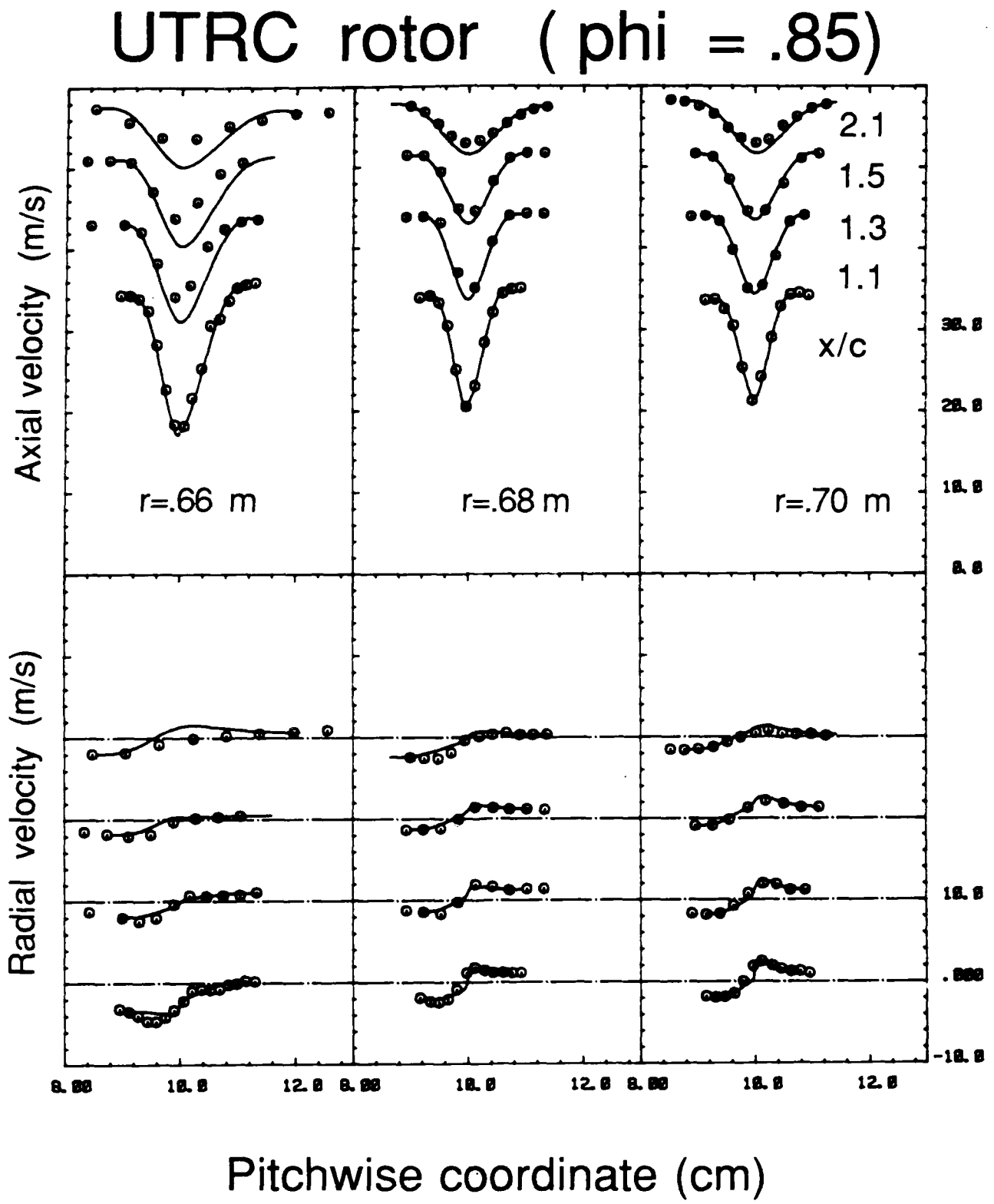

Figure 12.9 : Meridional and radial velocities in the UTRC rotor at a flow coefficient of 0.85
solid line : computation (De Ruyck and Hirsch, 1987)
squares : experiment (Dringg et al., 1982)

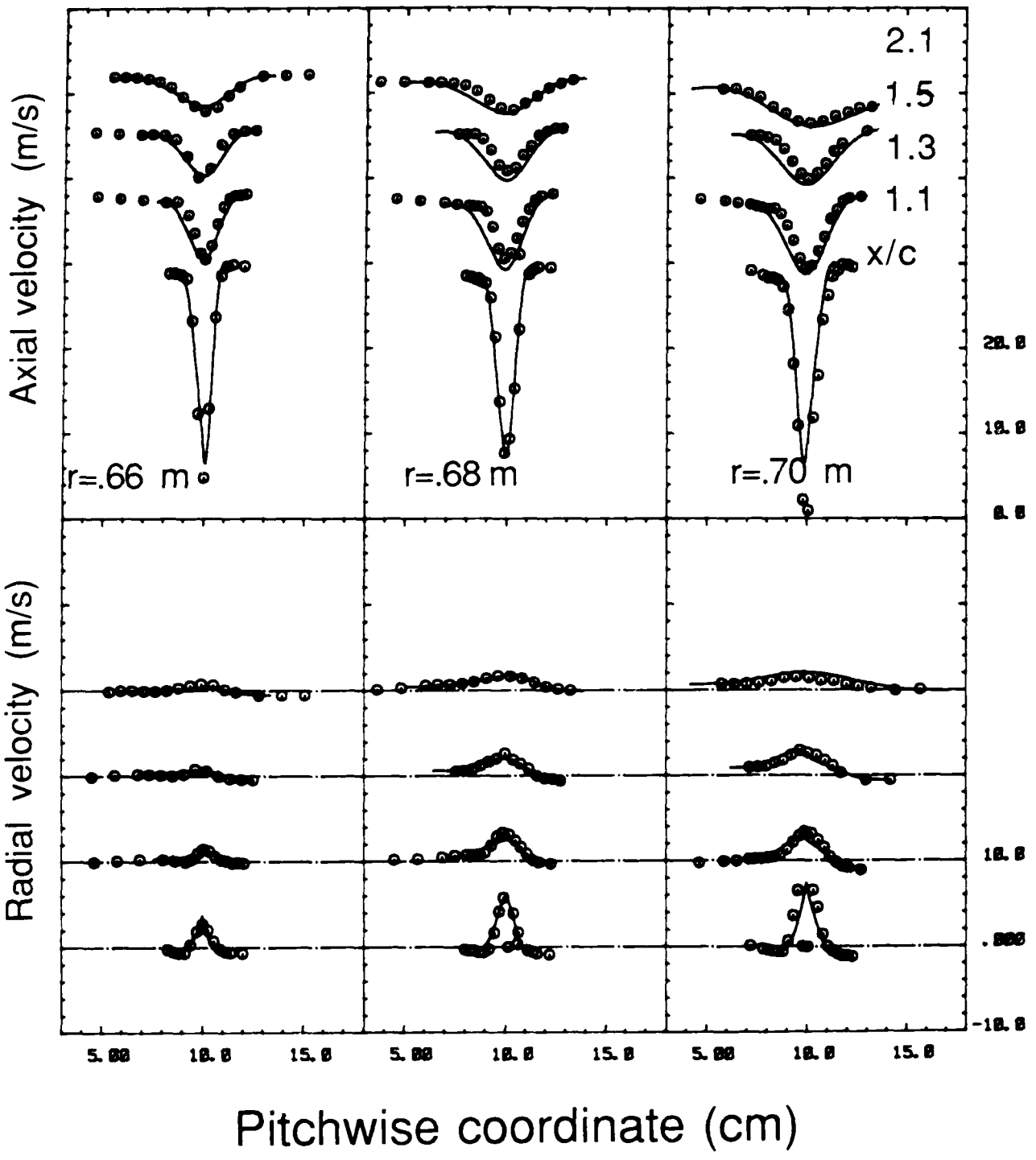

Figure 12.10 : Meridional and radial velocities in the UTRC rotor at a flow coefficient of 0.65
solid line : computation (De Ruyck and Hirsch, 1987)
squares : experiment (Dring et al., 1982)

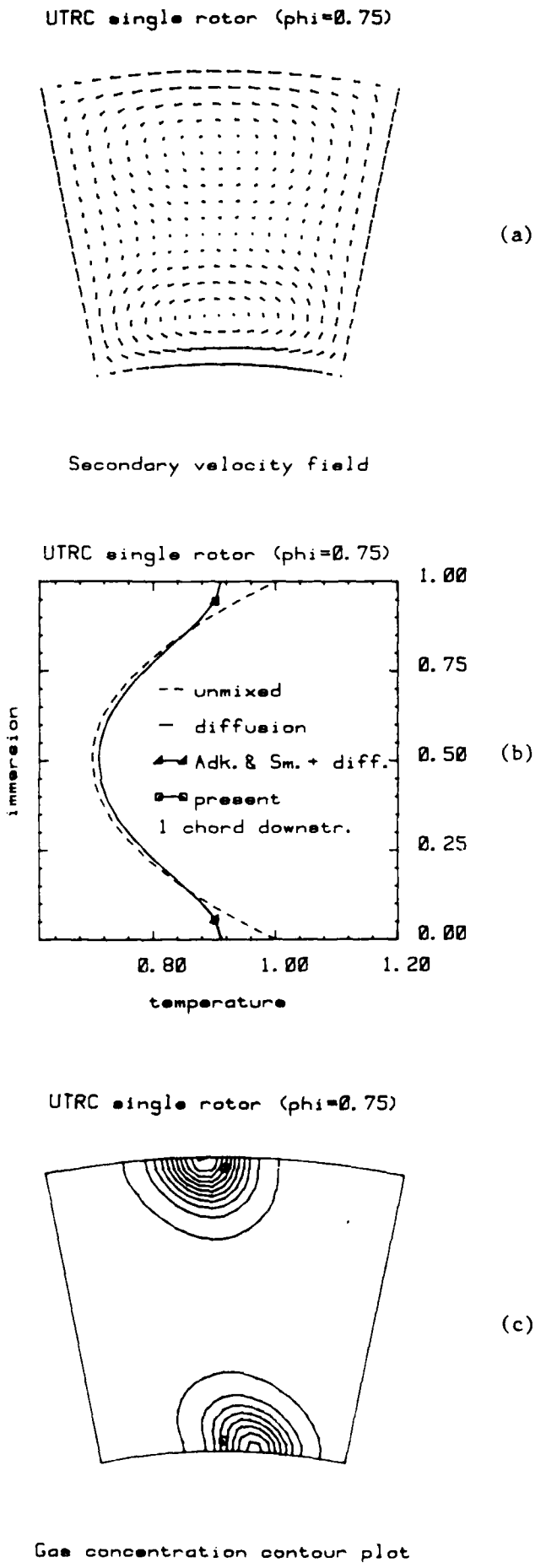

Figure 12.11 : Secondary flow field and radial redistributions, UTRC rotor 1 chord distance downstream of the trailing edge

UTRC single rotor (phi=0.75)

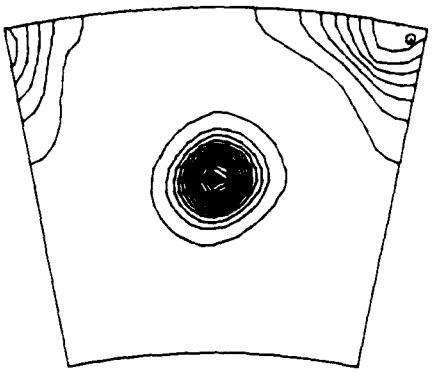

(a)

Gas concentration contour plot

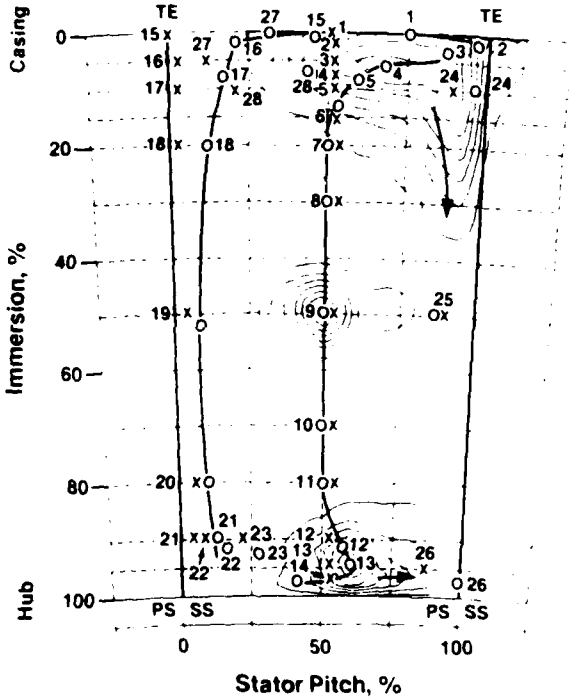

(b)

Figure 12.12 : Anisotropic diffusion experiments from Wisler et al. (1987) computation in the UTRC rotor

CONCLUSIONS

A complete secondary flow and radial mixing procedure has been presented. The secondary flows are found from a passage averaged vorticity equation for the main passage flow, and from integral methods in the boundary layers and wakes. Some modeling is used to reconstruct global secondary flow patterns. With the assumptions of the model, there is only one empirical constant to be determined, namely the turbulent diffusivity coefficient. Some additional work is required to validate theoretical formulations for the coefficient ε_t. The formula suggested by Gallimore and Cumpsty (1986) might be a valid first guess.

The radial redistributions of temperature or gas concentrations are fully computed from the transport equation, which makes the simulation of gas injections possible. Comparisons are made with the mixing approach of Adkins and Smith (1982).

Mixing effects have been computed in three different situations : a linear cascade where the secondary flows are mainly due to end-wall boundary layer effects, a rotor where unwisted blades yield an important non-free vortex flow, and a rotor which is representative for engineering applications. The mixing observed at the trailing edges is not very important and at least one chord distance downstream of the trailing edge is required to have significant redistributions. Turbulent diffusion appears to be important, whereas the secondary flow convection is significant in the case of strong non-free vortex behaviour (untwisted blades), or when the blade loading becomes very important (54° deflection). In general, convective effects are observed when the overall radial flow velocities exceed about 5% of the main flow velocities, and rapidly increase at higher values (ONERA test case). Convective effects can in general not be simulated by a diffusion type equation.

Although the turbulent mixing is more important in the viscous layers than elsewhere, turbulent mixing coefficients observed in the wakes can be considered as representative for the overall turbulent mixing effects.

In the future, the present theory is to be validated in complete multistage machines. It will be inserted in a Quasi-3D code where it will interact with the meridional and blade-to-blade computations. The redistribution of the total temperature can be computed axial station by axial station and redistributed pressures can next be found by considering the redistribution as an isentropic (or polytropic ?) process. In such a code it is possible to introduce some simplifications :

i) The profile boundary layer thicknesses can be found from available blade loss correlations rather than from the integral method proposed here.

ii) If the Quasi-3D code has a poisson solver, the secondary flow velocities are no more to be reconstructed from equation 5.1, but can be found by solving

$$\Delta\psi = \omega$$

where

$$w_{r.sec} = \frac{1}{r}\frac{\partial \psi}{\partial \theta}$$

$$w_{\theta.sec} = \frac{\partial \psi}{\partial r}$$

REFERENCES

ADKINS G.G., SMITH L.H., 1982, "Spanwise Mixing in Axial-Flow Turbomachines" ASME J. of Eng. for Power, vol 104, pp 97-110.

BEHLKE R.F., BURDSALL E.A., CANAL E.Jr, Korn N.D.,"Core Compressor Exit Stage Study - II. Final report", NASA CR-159812, PWA-5561-66, 1979.

BURDSALL E.A., CANAL E.Jr., LYONS K.A., "Core Compressor Exit Stage Study - I. Aerodynamic and Mechanical Design", NASA CR-159714, PWA-5561-55, 1979.

CAME P.M., MARSH H., "Secondary Flow in Cascades : two Simple Derivations for the Components of Vorticity", Jl. Mech. Eng. Sci., Vol 16, No 6, pp 391-401, 1974.

CARTER, COHEN, 1946, "Preliminary Investigation into the Three-Dimensional Flow through a Cascade of Aerofoils", Aero. Res. Council, R & M 2336, 1946.

COOKE, HALL, 1962, "Boundary Layers in Three Dimensions" Progress in Aeronautical Sciences, Vol 2, Boundary Layer Problems, Pergamon.

DE RUYCK J., 1982, "Computation of End-Wall Boundary Layers in Axial Compressors" Phd Thesis, Vrije Universiteit Brussel, Dept of Fluid Mechanics.

DE RUYCK J., HIRSCH C., 1981, "Investigations of an Axial Compressor End-Wall Boundary Layer Prediction Method" ASME Journal of Eng. for Power, Vol 103, no 1, pp 20-33, 1981

DE RUYCK J., HIRSCH C., 1983, "End-Wall Boundary Layers in Multistage Axial Compressors" AGARD 61 th Specialist Meeting, Viscous Effects in Turbomachines, CP 351.

DE RUYCK J., HIRSCH C., 1987a, "Radial Mixing in Turbomachines" report VUB-TN-39, Vrije Universiteit Brussel, Dept. of Fluid Mechanics,

DE RUYCK J., HIRSCH C., 1987b, "Radial Mixing in Turbomachines" report VUB-TN-40, Vrije Universiteit Brussel, Dept. of Fluid Mechanics,

DIXON S.L., 1974, "Secondary Vorticity in Axial Compressor Blade Rows" Nasa Sp304.

DRING R.P., JOSLYN H.D., HARDIN L.W., 1982, "An Investigation of Axial Compressor Rotor Aerodynamics" ASME J. Eng. for Power, vol 104, pp 84-94, jan 1982.

GALLIMORE S.J., CUMPSTY N.A., 1986a "Spanwise Mixing in Multistage Axial

Flow Compressors : Part I - Experimental Investigation" ASME paper 86-GT-20, 1986

GALLIMORE S.J., 1986b "Spanwise Mixing in Multistage Axial Flow Compressors : Part II - Throughflow Calculations Including Mixing" ASME paper 86-GT-21.

HAH C., LAKSHMINARAYANA B., "Prediction of Two- and Three- Dimensional Asymmetrical Turbulent Wakes, Including Curvature and Rotation Effects" AIAA Journal Vol 18, No 10, 79-1561, 1979.

HAWTHORNE W.R., 1951, "Secondary Circulation in Fluid Flow" Proc. Roy. Soc. Vol a, no 209, pp 374-397.

HAWTHORNE W.R., "Rotational flow through Cascades" Q. Jl. Mech. appl. Math. Vol 8, part 3, pp 266-292, 1955.

HIRSCH C., DRING R.P., 1987, "Through Flow Models for Mass and Momentum Averaged Variables" Trans. ASME, Journal of Turbomachinery, vol 109, pp 362-370, 1987

HIRSCH C., WARZEE G., 1979, "An Integrated Quasi-3D Finite Element Calculation Program for Turbomachinery flows" ASME Journal of Engineering for Power, Vol 101, pp 141-148.

HORLOCK J.H., 1971, "Cross Flows in Bounded Three Dimensional Turbulent Boundary Layers" Cambridge U., Cued/a -; Turbo/tr28.

HORLOCK J.H., PERKINS H.J., 1974, "Annulus Wall Boundary Layers in Turbomachines" Agard ag 185.

KOCH C.C., SMITH L.H., Jr., 1976, "Loss Sources and Magnitudes in Axial-Flow Compressors" ASME, J. of Engineering for Power, July 1976, pp. 411-424.

KORKAN K.D., PETRIE S.L., GASPERAS G., 1977 "A Unified Theory of the Two Dimensional ans Axisymmetric Laminar, Transition and Turbulent Wake Process Utililizing the Integral Technique", AIAA paper 77-708.

LAKSHMINARAYANA B., POPOVSKI P. "Three-Dimensional Boundary Layer on a Compressor Rotor Blade at Peak Pressure Rise Coefficient" ASME Journal of Turbomachinery, Vol 109, pp 91-98, january 1987.

LARGUIER R., 1980, "Experimental Analysis Methods for Unsteady Flows in Turbomachines" Measurement Methods in Rotating Components of Turbomachinery, P71, ASME.

MELLOR G.M., WOOD G.L., 1971, "An Axial Compressor End-Wall Boundary Layer Theory" ASME Journal of Basic Engineering, Series d, Vol 93, pp 300-316.

RAVINDRANATH A., LAKSHMINARAYANA B., "Mean Velocity and Decay Characteristics of the Near and Far Wake of a Compressor Rotor Blade of Moderate Loading" Trans. ASME, Journal of Engineering for Power, Vol 102, pp 535-548, 1980.

REYNOLDS B., LAKSHMINARAYANA B., "Characteristics of Lightly Loaded Fan Rotor Blade Wakes" NASA CR-3188, 1979.

SCHLICHTING H., "Boundary Layer Theory" McGrew Hill, New York, 1955

SMITH L.H., 1955, "Secondary Flow in Axial-Flow Turbomachinery" Trans. ASME, Vol 77, no 7, p 1065.

SMITH A.G., 1957, "On the Generation of the Streamwise Component of Vorticity for Flows in Rotating Passages" Aeronaut. Quart. 8 : 369.

SMITH L.H., 1969, "Casing Boundary Layers in Multistage Axial Flow Compressors" Brown Boveri Symposium, Flow Research on Blading, Elsevier.

SQUIRE H.B., WINTER K.G. "The Secondary Flow in a Cascade of Airfoils in a Nonuniform Stream" Journal of Aeronaut. Sc., Vol 18, p271, 1951.

WHITFIELD C.W., KEITH J.S., "Spanwise Redistribution of Energy and Loss in an Axial Flow Compressor by Wake Centrifugation", Wright Patterson Air Force Base, OHIO 45433, Final report AFWAL-TR-84-2109, 1985.

WISLER D.C., BAUER R.C., OKIISHI T.H., "Secondary Flow, Turbulent Diffusion and Mixing in Axial-Flow Compressors", ASME paper 87-GT-16, 1987

APPENDIX A : MERIDIONAL COORDINATE SYSTEM

A.1 Some notions of curvature

In the present appendix some notions of curvature are reviewed and applied to the vector operations such as divergence and rotation.

It can be shown that in each orthogonal coordinate system, a set of coordinates x_1, x_2, x_3 with unit vectors e_1, e_2, e_3 can be defined in such a way that all the surfaces x_1=cte, x_2=cte, x_3=cte intersect in three orthogonal curves. x_1, x_2 and x_3, as well as their dimensions, are a priori unknown functions, except for special cases of orthogonal coordinates. In a cylindrical coordinate system for example, x_1, x_2, x_3 are found to be x, r, θ with as dimensions L,L,1.

The length δl_i along the coordinate line δx_i is by definition given by

$$\delta l_i = h_i \delta x_i \tag{A.1}$$

where h_1, h_2, h_3 are the lame or metric coefficients, which are also a priori unknown functions (e.g. the cylindrical coordinate system : $h_1=h_2=1$, $h_3=r$)

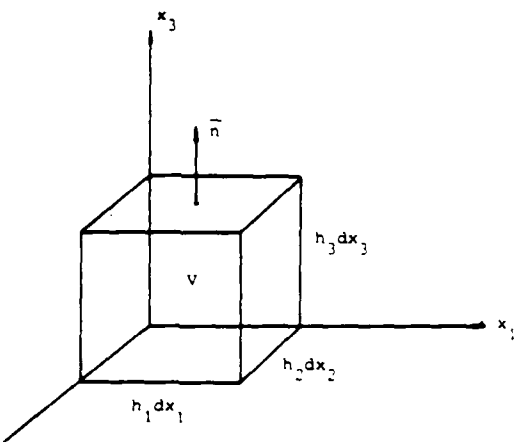

Figure A.1 : Elementary volume in curvilinear coordinates

The gradient operation can easily be expressed in a curvilinear coordinate system, since from

$$\frac{\partial \phi}{\partial n} = \vec{1}_n (\vec{\nabla} \phi) \tag{A.2}$$

from fig A.2 that for example

$$\frac{1}{h_2}\frac{\partial \vec{e}_1}{\partial x_2} = -\frac{1}{R_{21}}\vec{e}_2 \tag{A.10}$$

where R_{21} is the radius of curvature of the plane curve obtained by intersection of the surface x_1=cte with the plane $(\vec{e}_1, \delta\vec{e}_1)$, or $(\vec{e}_1, \vec{e}_2)$ (fig A.2). According to the theorem of Meusnier, this radius of curvature can be related to R_2, the principal radius of curvature of x_2 through (fig A.2)

$$R_{21} = \frac{R_2}{\cos\theta_{21}} \tag{A.11}$$

θ_{21} is the angle between e_1 and the principal normal of x_2.

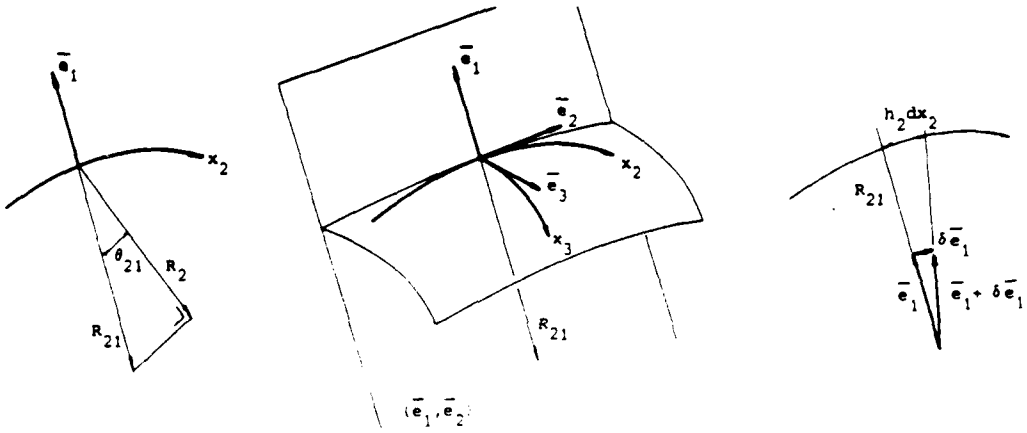

Figure A.2 : Radii of curvature in curvilinear coordinates

From eqs A.7 and A.10 repeated for each R_{ij} it can be shown that e.g. for e_1

$$\frac{1}{h_1}\frac{\partial \vec{e}_1}{\partial x_1} = \frac{1}{R_{12}}\vec{e}_2 + \frac{1}{R_{13}}\vec{e}_3 \tag{A.12}$$

$$\vec{\nabla}\vec{e}_1 = -\frac{1}{R_{21}} - \frac{1}{R_{31}} \quad . \tag{A.13}$$

Hence, if all the radii R_{ij} are known functions, the correction terms in eqs A.8 and A.9 are known, while the functions x_i and h_i can -principally- be determined from

$$\frac{1}{R_{ij}} = -\frac{1}{h_i h_j}\frac{\partial h_i}{\partial x_j} \qquad (A.14)$$

A.2 The meridional coordinate system

The meridional coordinate system is illustrated on fig 3.1. In general curvature is present in both circumferential and meridional directions. The corresponding coordinates are m,n,u where m denotes the meridional direction, n the direction normal to the end-wall and u is the pitchwise direction. m, n and u are defined as lengths. The independent coordinates are denoted as x_m, x_n and x_u and the corresponding metric coefficients as h_m, h_n, h_u.

The direction u is taken positive in the direction normal to the profile walls, while n is always taken positive from the hub wall. Hence, if the pressure side coordinate system is right handed, the suction side coordinate system will be left handed, and vice-versa.

According to the theorem of Dupin, the system of coordinates m,n,u is an orthogonal coordinate system, since the m and u lines are lines of principal curvature. A rigorous development in non-orthogonal streamline coordinates is not considered.

The different radii of curvature of the coordinate lines along the blade profiles are found to be (fig 3.1)

$$\frac{1}{R_{mn}} = \frac{1}{R_m} = +\frac{\partial\sigma}{\partial m}\bigg|_n \qquad (A.15)$$

$$\frac{1}{R_{mu}} = 0 \qquad (A.16)$$

$$\frac{1}{R_{nm}} = \frac{1}{R_n} = -\frac{\partial\sigma}{\partial n}\bigg|_m \qquad (A.17)$$

$$\frac{1}{R_{nu}} = 0 \qquad (A.18)$$

$$\frac{1}{R_{um}} = -\frac{1}{r}\frac{\partial r}{\partial m}\bigg|_n = -\frac{\sin\sigma}{r} \qquad (A.19)$$

$$\frac{1}{R_{un}} = -\frac{1}{r}\frac{\partial r}{\partial n}\bigg|_m = -\frac{\cos\sigma}{r} \qquad (A.20)$$

According to section A.1, the knowledge of these radii allows the application of any vector operation in the meridional coordinate system.

From eqs (A.14), (A.19) and (A.20), it follows that

$$x_u = \theta \tag{A.21}$$

$$h_u = r \tag{A.22}$$

h_m, h_n, x_m and x_n cannot be determined explicitly for an arbitrary wall shape. Due to axisymmetry, it however follows from eqs (A.14), (A.16) and (A.18) that

$$\frac{\partial h_m}{\partial x_u} = \frac{\partial h_n}{\partial x_u} = 0 \tag{A.23}$$

It is to be observed that eqs (A.15) to (A.20) are valid in both pressure and suction side m,n,u coordinate systems which are respectively right and left handed or vice-versa. Care must be taken when chosing the sign convention of σ.

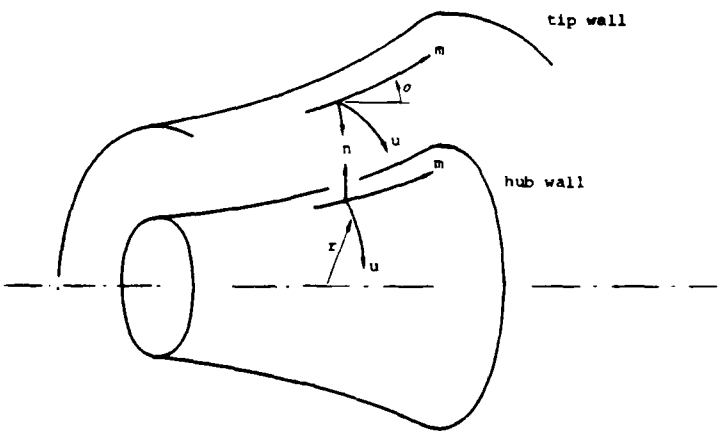

figure A.3 : meridional coordinate system

APPENDIX B : MAIN SECONDARY FLOW EQUATION

The incompressible inviscid vorticity equation can be written as

$$(\vec{W}.\vec{\nabla}).\vec{\omega} - (\vec{\omega}.\vec{\nabla}).\vec{W} = 0 \tag{B.1}$$

The vorticity component in the n direction (see figure A.3) will directly be assumed to be zero which means that the blade to blade flow is considered to be a potential flow.

$$\omega_n = \frac{1}{r}\frac{\partial w_m}{\partial \theta} - \frac{1}{r}\frac{\partial r w_u}{\partial m} = 0 \tag{B.2}$$

integration of eq (B.2) from pressure to suction side yields

$$\frac{1}{s}\Delta w_m = \frac{1}{r}\frac{\partial}{\partial m}\bar{rw}_u - \frac{tg\beta}{s}\Delta w_u \tag{B.3}$$

Δw_m represents the difference in meridional velocity between suction and pressure side of the blade (fig D.1). s denotes the pitch. Taking the following boundary condition into account

$$w_u\big|_{blade} = tg\beta\, w_m\big|_{blade}$$

eq (B.3) becomes

$$\frac{1}{s}\Delta w_m = \cos^2\beta\,\frac{1}{r}\frac{\partial}{\partial m}(\bar{rw}_u) \tag{B.4}$$

The projection of equation (B.1) in the direction u is of no concern. The projection in direction m yields (see appendix A)

$$\begin{aligned} &w_m\frac{\partial \omega_m}{\partial m} + w_n\frac{\partial \omega_m}{\partial n} + w_u\frac{\partial \omega_m}{\partial u} + \omega_n\left(\frac{w_n}{R_{nm}} - \frac{w_m}{R_{mn}}\right) + \omega_u\left(\frac{w_u}{R_{um}} - \frac{w_m}{R_{mu}}\right) \\ &= \omega_m\frac{\partial w_m}{\partial m} + \omega_n\frac{\partial w_m}{\partial n} + \omega_u\frac{\partial w_m}{\partial u} + w_n\left(\frac{\omega_n}{R_{nm}} - \frac{\omega_m}{R_{mn}}\right) + w_u\left(\frac{\omega_u}{R_{um}} - \frac{\omega_m}{R_{mu}}\right) \end{aligned} \tag{B.5}$$

R_{ij} are the radii of curvature of the m,n,u lines (see appendix A). Expressing that

$$\omega_n = 0$$
$$R_{mu} = 0 \qquad \text{(B.6)}$$
$$R_{nm} = 0$$

one finds

$$w_m \frac{\partial}{\partial m} \omega_m + w_n \frac{\partial}{\partial n} \omega_m + w_u \frac{\partial}{\partial u} \omega_m + \omega_u \frac{w_u}{R_{um}}$$
$$= \omega_m \frac{\partial}{\partial m} w_m + \omega_u \frac{\partial}{\partial u} w_m - w_n \frac{\omega_m}{R_{mn}} + w_u \frac{\omega_u}{R_{um}} \qquad \text{(B.7)}$$

Pitch averaging of this equation yields

$$\bar{w}_m\left[\frac{\partial}{\partial m} \tilde{\omega}_m - \frac{tg\beta}{s} \Delta\omega_m\right] + \bar{w}_n\left[\frac{\partial}{\partial n} \tilde{\omega}_m - \frac{tg\eta}{s} \Delta\omega_m\right] + \bar{w}_u \frac{1}{s} \Delta\omega_m + \bar{\omega}_u \bar{w}_u / R_{um}$$
$$= \bar{\omega}_m\left[\frac{\partial}{\partial m} \tilde{w}_m - \frac{tg\beta}{s} \Delta w_m\right] + \bar{\omega}_u \frac{1}{s} \Delta \bar{w}_m + \bar{\omega}_u \bar{w}_u / R_{um} - \bar{\omega}_m \bar{w}_n / R_{mn} \qquad \text{(B.8)}$$

Second order fluctuations have been neglected. η is the radial blade inclination angle which can be assumed to be very small. Assuming $\tilde{w}_n \ll \tilde{w}_m$ equ (B.8) reduces to

$$\bar{w}_m \frac{\partial}{\partial m} \tilde{\omega}_m = \bar{\omega}_m \frac{\partial}{\partial m} \tilde{w}_m + (\tilde{\omega}_u - tg\beta\, \tilde{\omega}_m) \frac{1}{s} \Delta w_m$$
$$- (\tilde{w}_u - tg\beta\, \tilde{w}_m) \frac{1}{s} \Delta\omega_m \qquad \text{(B.9)}$$

The second term in the r.h.s. arises from the presence of a mainflow velocity gradient ($\tilde{\omega}_u$) in presence of a flow deflection (Δw_m, eq (B.4)). $\Delta\omega_m$ can be found from

$$\Delta\omega_m = \frac{1}{r} \frac{\partial}{\partial n} r\Delta w_u - \frac{\partial}{\partial u} \Delta w_n \approx \frac{1}{r} \frac{\partial}{\partial n} r\Delta w_u \qquad \text{(B.10)}$$

This last contribution results from changes in circulation along the blades, since from (B.3) and (B.4)

$$\frac{1}{r} \frac{\partial}{\partial n} r\Delta w_u = \frac{1}{r} \frac{\partial}{\partial n} \left(s \sin\beta \cos\beta \frac{\partial}{\partial m} r\tilde{w}_u\right) \qquad \text{(B.11)}$$

Equation B.10 is rigorous when the radial velocity is antisymmetric with u, as will be assumed.

The averages of ω_m and ω_u are given by (metric coefficients are constant with x_u)

$$\omega_m = \frac{1}{r}\frac{\partial r w_u}{\partial n} - \frac{1}{r}\frac{\partial w_n}{\partial \theta}$$

$$\tilde{\omega}_m = \frac{1}{r}\frac{\partial}{\partial n} r\tilde{w}_u - \frac{1}{s}\Delta w_n \qquad \text{(B.12)}$$

$$\omega_u = \frac{\partial w_n}{\partial m} - \frac{\partial w_m}{\partial n}$$

$$\tilde{\omega}_u = \frac{\partial}{\partial m}\tilde{w}_n - \frac{tg\beta}{s}\Delta w_n - \frac{\partial}{\partial n}\tilde{w}_m + \frac{tg\eta}{s}\Delta w_m + \frac{\tilde{w}_m}{R_{mn}} \qquad \text{(B.13)}$$

$1/R_{nm}$ was assumed to be small.

APPENDIX C : END-WALL BOUNDARY LAYER COMPUTATIONS

The End-wall boundary theory presently used has been presented extensively in (De Ruyck and Hirsch, 1981, 1983) and is briefly summarized below.

The basic equations are written in the meridional coordinate system m,n,u (fig A.3). 'c' denotes an absolute velocity and 'w' a relative velocity component.

The boundary layer momentum and entrainment equations are

$$\frac{d}{dm}\rho r c_m^2 \theta_{mm} + \rho r c_m \delta_m^* \frac{dc_m}{dm} - \rho c_m^2 \sin\sigma\,(\delta_u^* tg\alpha + \theta_{uu}) = r\tau_m + rF_m \qquad \text{(C.1)}$$

$$\frac{d}{dm}\rho r c_m^2 \theta_{um} + \rho r c_m \delta_m^* \frac{dc_u}{dm} + \rho c_m^2 \sin\sigma\,(\delta_m^* tg\alpha + \theta_{um}) = r\tau_u + rF_u \qquad \text{(C.2)}$$

$$\frac{1}{r\rho c_m}\ \frac{d}{dm}\ r\rho c_m(\delta - \delta_m^*) = \frac{E(H_k^*)}{\cos\alpha} \qquad (C.3)$$

Eqs (C.1) to (C.3) are written in the absolute reference system. The boundary layer thicknesses in these equations are defined as

$$\theta_{ij} = \int_o^\delta \left(\frac{\hat{w}_i}{w_m} - \frac{w_i}{w_m} \right) \frac{\rho w_j}{\rho w_m}\, dn \qquad (C.4)$$

$$\delta_i^* = \int_o^\delta \left(\frac{\hat{\rho w}_i}{\rho w_m} - \frac{\rho w_i}{\rho w_m} \right) dn \qquad (C.5)$$

These thicknesses are defined in the wall reference system. The velocities with an overhead carat (^) denote the 'outer' or 'inviscid' reference velocities. Corrections for variations of these 'inviscid' values with the distance from the wall are not considered [2]. The velocity ratios are modelled through (figure C.1)

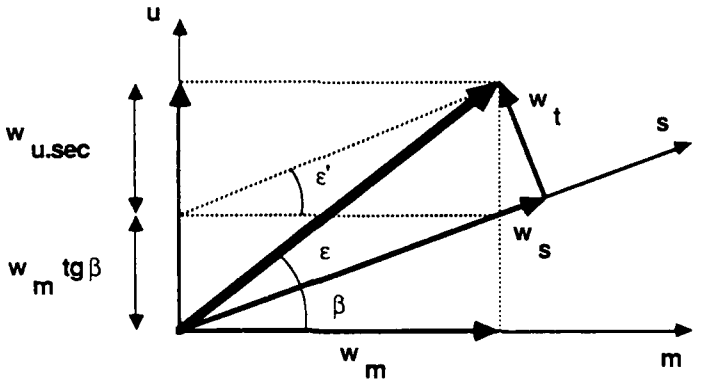

Figure C.1 : velocity components

$$\frac{w_m}{w_m} = 1 - b\left(1 - \frac{n}{\delta}\right)^n \qquad (C.6)$$

$$\frac{w_{u.sec.ewbl}}{\hat{w}_m} = \frac{w_u - w_m tg\alpha}{\hat{w}_m} = (1-b)tg\varepsilon'_w\left(1 - \frac{n}{\delta}\right)^n \qquad (C.7)$$

where

$$b = \exp(-10n\, C_f^{.5}\, \cos\beta^{-.134}) \qquad (C.8)$$

$$tg\varepsilon'_w = tg(\varepsilon_w + \beta) - tg\beta \qquad (C.9)$$

The density ratio is given by

$$\frac{\rho}{\hat{\rho}} = 1 - 2a\left(1 - \frac{w_m}{\hat{w}_m}\right) + a(1+4a)\left(1 - \frac{w_m}{\hat{w}_m}\right)^2 \qquad (C.10)$$

$$a = .89\,\frac{\gamma-1}{2}\,M_e^2 \qquad (C.11)$$

The entrainment rate E is given by

$$E(H_k^*) = 0.0306\,(H_k^* - 3.)^{0.653} \qquad (C.12)$$

$$H_k^* = \frac{\delta - \delta_{mk}^*}{\theta_{mmk}} \qquad (C.13)$$

The mainstream and cross flow shear stresses are obtained from

$$\tau_s = C_f \frac{\rho \hat{w}_s^2}{2} \qquad (C.14)$$

$$\tau_t = \tau_s tg\varepsilon_w \qquad (C.15)$$

where

$$C_f = 0.246\, Re_{\theta_{mm}}^{-0.268}\left(\frac{\hat{T}}{T^*}\right)\exp(-1.56\, H_k) \qquad (C.16)$$

$$H_k = \frac{\delta_{mk}^*}{\theta_{mmk}} \qquad (C.17)$$

$$\frac{T^*}{\hat{T}} = 1 + 0.72\, a$$

The 'kinematic' thicknesses δ^*_{mk} and θ_{mmk} are defined as

$$\delta^*_{mk} = \int_o^\delta \left(1 - \frac{w_m}{\hat{w}_m}\right) dn \tag{C.18}$$

$$\theta_{mmk} = \int_o^\delta \left(1 - \frac{w_m}{\hat{w}_m}\right) \frac{w_m}{\hat{w}_m} dn \tag{C.19}$$

Eqs (C.4) to (C.19) are written in the wall reference system. The thicknesses θ_{mm}, θ_{um}, δ^* and δ^*_u and the parameters b and n have the same values in both absolute and relative systems whereas the wall skewing angles and θ_{uu} are related by the jump relations

$$(tg\varepsilon'_w)^{abs} = (tg\varepsilon'_w)^{rel} + \frac{1}{1-b}\left(tg\beta^{rel} - tg\beta^{abs}\right)$$

$$\theta^{abs}_{uu} = \theta^{rel}_{uu} + U\delta^*_u/\hat{c}_m \tag{C.20}$$

The blade mainstream defect force is found from

$$\frac{F_s}{\rho} = L \frac{\hat{w}_s^2}{2\cos\gamma}\, \sigma\, C_L^2 \qquad L \approx .01 \tag{C.21}$$

The tranverse lift defect is found from

$$\frac{F_t}{\rho} = -\frac{k}{s} w_s^2 \theta_{tm} \tag{C.23}$$

in absence of a tip clearance and from

$$\frac{F_t}{\rho} = \frac{t_c}{\cos\alpha} w_m \frac{dw_u}{dm} - \frac{k'}{s} w_s^2 \theta_{tm} \tag{C.24}$$

in presence of a tip clearance. The constants k and k' are given by

$$k \approx 3. \qquad k' \approx .5 \tag{C.25}$$

The cross flow thickness is defined through

$$\theta_{tm} = -\cos\alpha \int_o^\delta \frac{w_t}{w_s} \frac{w_m}{w_s} dn$$

$$\theta_{tm} = (\theta_{um} - \theta_{mm} tg\beta) \cos^2\beta \qquad (C.26)$$

Eqs (C.21) to (C.26) are written in the blade reference system.

The basic eqs (C.1), (C.2) and (C.3) are integrated in the meridional direction using a fifth order Runge-Kutta method with as complementary relations eqs (C.4) to (C.26). The amount of secondary flow is given by the pitch-averaged cross momentum and displacement thicknesses, which will be used as input in the next radial flow computations (section 5).

APPENDIX D : INTEGRAL BOUNDARY LAYER EQUATIONS IN MERIDIONAL COORDINATES

In the following, the flow variables denoted with a carat ^ are those obtained from the quasi 3D computations. The integral boundary layer approach seeks for the differences between these variables and the real flow variables. The momentum equations will be derived taking wall curvature and variable inviscid flow parameters into account.

Both real and inviscid flow satisfy momentum conservation. Subtraction of both conservation laws yields

$$\hat{\rho}(\hat{\vec{W}}\hat{\vec{\nabla}})\hat{\vec{W}} - \rho(\vec{W}\vec{\nabla})\vec{W} + 2\vec{\omega}\Lambda(\hat{\rho}\hat{\vec{W}}-\rho\vec{W}) = -\vec{\nabla}(\hat{p}-p) + \vec{\nabla}(-\bar{\bar{\tau}}) \qquad (D.1)$$

Through the use of inviscid flow parameters as reference ones, radial equilibrium is taken into account inside the PBL.

The m and n projections of the integral boundary layer momentum equation are found to be, after considerable manipulation (De Ruyck and Hirsch, 1987, first interim report) :

$$\frac{\partial}{\partial m}\rho w_m^2(\theta_{mm} - \lambda_{mm}) + \rho w_m \delta_m^* \frac{\partial w_m}{\partial m}$$

$$+ \frac{\partial}{\partial n}\rho w_m^2(\theta_{mn} - \lambda_{mn}) + \rho w_m \delta_n^* \frac{\partial w_m}{\partial n} \qquad (D.2)$$

$$+ \frac{1}{R_{nm}}\rho w_m^2 I_{nn} + \frac{1}{R_{um}}\rho w_m^2 I_{uu} - \frac{1}{R_{mn}}\rho w_m^2 I_{mn} \pm 2\omega \frac{r}{R_{um}}\hat{\rho w}_m \delta_u^*$$

$$= \tau_s$$

$$\frac{\partial}{\partial m}\rho w_m^2(\theta_{nm}-\lambda_{nm}) + \rho w_m\delta_m^*\frac{\partial w_n}{\partial m}$$

$$+\frac{\partial}{\partial n}\rho w_m^2(\theta_{nn}-\lambda_{nn}) + \rho w_m\delta_n^*\frac{\partial w_n}{\partial n} \qquad (D.3)$$

$$-\frac{1}{R_{nm}}\rho w_m^2 I_{mn} + \frac{1}{R_{un}}\rho w_m^2 I_{uu} + \frac{1}{R_{mn}}\rho w_m^2 I_{mm} \pm 2\omega\frac{r}{R_{un}}\hat{\rho w}_m\delta_u^* = \tau_n$$

where following thickness definitions are found

$$(\hat{\rho w}_m^2)_w\theta_{ij} = \int_o^\delta(\hat{w}_i - w_i)\rho w_j r d\theta \qquad (D.4)$$

$$(\hat{\rho w}_m^2)_w\lambda_{ij} = \int_o^\delta(\hat{w}_{iw} - \hat{w}_i)(\hat{\rho w}_j - \rho w_j)\, r d\theta \qquad (D.5)$$

$$(\hat{\rho w}_m)_w\delta_i^* = \int_o^\delta(\hat{\rho w}_i - \rho w_i)\, r d\theta \qquad (D.6)$$

$$(\hat{\rho w}_m^2)_w I_{ij} = \int_o^\delta(\hat{\rho w}_i\hat{w}_j - \rho w_i w_j)\, r d\theta \qquad (D.7)$$

The ± in equations (D.2) and (D.3) indicate right or left hand coordinates. The + sign is selected when taking w_u always positive in the rotation sense. The thicknesses λ_{ij} which appear in eqs (D.2) and (D.3) originate from variations in velocity $\hat{w}$. These terms are of second order since these variations are in general small and their contribution will not be considered. Neglecting λ_{ij} reduces these equations to, after some manipulations

$$\frac{\partial}{\partial m}\rho w_m^2\theta_{mm} + \frac{\partial}{\partial n}\rho w_m^2\theta_{mn} + \rho w_m\delta_m^*\partial_m w_m + \rho w_m\delta_n^*\partial_n w_m$$

$$+\frac{1}{R_{nm}}\rho w_m\left(w_m\theta_{nn} - w_m\theta_{mm} + w_n\delta_n^*\right) - \frac{1}{R_{mn}}\rho w_m^2\left(2\theta_{mn} + \delta_n^*\right) \qquad (D.8)$$

$$+\frac{1}{R_{um}}\rho w_u\left(w_u(\theta_{mm} + \delta_m^*) + 2U\delta_m^*\right) = \tau_s$$

$$\frac{\partial}{\partial m}\rho w_m^2\theta_{nm} + \frac{\partial}{\partial n}\rho w_m^2\theta_{nn} + \rho w_m\delta_m^*\partial_m w_n + \rho w_m\delta_n^*\partial_n w_n$$

$$+ \frac{1}{R_{mn}}\rho w_m^2(\theta_{mm} + \delta_m^* - \theta_{nn}) - \frac{1}{R_{nm}}\rho w_m(2w_m\theta_{nm} + w_n\delta_m^*) \qquad (D.9)$$

$$+ \frac{1}{R_{un}}\rho w_u(w_u(\theta_{mm} + \delta_m^*) + U\delta^*) = \tau_n$$

All the variables are written in the right handed blade reference coordinate system and

$$U = \omega r \quad \text{in a rotor}$$
$$U = 0 \quad \text{in a stator}$$

For all approximations made when obtaining eqs (D.8) and (D.9) it is refered to appendix B.

Eqs (D.8) and (D.9) are to be written in the blade reference system since they are constructed from the steady Navier-Stokes equations.

D.2 Entrainment and skin friction

The entrainment equation is constructed from the continuity as follows

$$\frac{\partial}{\partial x_m}h_n h_u \rho w_m + \frac{\partial}{\partial x_n}h_m h_u \rho w_n + \frac{\partial}{\partial x_u}h_m h_n \rho w_u = 0 \qquad (D.10)$$

Integration of eq (D.10) with respect to dx_u yields

$$\int_o^\delta \frac{\partial}{\partial x_m}(h_n h_u \rho w_m)dx_u + \int_o^\delta \frac{\partial}{\partial x_n}(h_m h_u \rho w_n)dx_u + [h_m h_n \rho w_u]_o^\delta = 0 \qquad (D.11)$$

Inverting integral and derivative, with $\partial h/\partial x_n = 0$ and $h\,dx_u = r d\theta$

$$\frac{\partial}{\partial x_m}h_n\int_o^\delta \rho w_m r d\theta - [h_n r\rho w_m \frac{\partial\delta}{\partial x_m}]_o^\delta$$

$$+ \frac{\partial}{\partial x_n}h_m\int_o^\delta \rho w_n r d\theta - [h_m r\rho w_n \frac{\partial\delta}{\partial x_n}]_o^\delta + [h_m h_n \rho w_u]_o^\delta = 0 \qquad (D.12)$$

Division by $h_m h_n$ and rearranging leads to

$$\frac{\partial}{\partial m}\int_o^\delta \rho w_m r d\theta - \frac{1}{R_{nm}}\int_o^\delta \rho w_m r d\theta - \rho w_m \frac{\partial \delta}{\partial m} + \rho w_m \frac{\delta}{R_{um}}$$

$$+ \frac{\partial}{\partial n}\int_o^\delta \rho w_n r d\theta - \frac{1}{R_{mn}}\int_o^\delta \rho w_n r d\theta - \rho w_n \frac{\partial \delta}{\partial n} + \rho w_n \frac{\delta}{R_{um}} = -[\rho w_u]_o^\delta \qquad (D.13)$$

which is easily rearranged to

$$\frac{\partial}{\partial m}\rho w_m(\delta-\delta_m^*) + \frac{\partial}{\partial n}\rho w_m(\delta-\delta_n^*) - \frac{1}{R_{nm}}\rho w_m(\delta-\delta_m^*) - \frac{1}{R_{mn}}\rho w_m(\delta-\delta_n^*)$$

$$+ \rho\delta\left(\frac{w_m}{R_{um}} + \frac{w_n}{R_{un}}\right) = \rho\left((\vec{W}\vec{\nabla})\delta - [w_u]_o^\delta\right) \qquad (D.14)$$

The last term is related to the entrainment rate E as follows, s being the streamline direction

$$\rho\left((\vec{W}\vec{\nabla})\delta - [w_u]_o^\delta\right) = \rho\frac{w_s}{\cos\alpha}\left(\frac{\partial\delta}{\partial s} - \frac{[w_u]_o^\delta}{W}\right)$$

$$= \rho\frac{w_s}{\cos\alpha\cos\beta}E \qquad (D.15)$$

Eq (D.15) is written in the relative coordinate system. The entrainment rate is given as an empirical function of Head's shape factor through :

$$E = 0.0306/(H^*-3.)^{.653} \qquad (D.16)$$

The validity of this empirical relation is questionable in presence of curved walls but no corrections to this equation are found in the open literature. Since it is however shown that curvature has a strong effect on the turbulence properties of the flow, it is believed that a correction should be introduced in eq (D.16). No attempts are made in the present work to correct eq (D.16) and this should be considered as a limitation in presence of strongly curved walls.

The estimation of the mainstream skin friction occurs through the use of a non dimensional skin friction coefficient generally denoted as C_f and defined through

$$\tau_s = C_f\rho\frac{\hat{w}_s^2}{2} \qquad (D.17)$$

Ludwig-Tillman's relation is generally accepted. This relation expresses C_f as function of the Reynolds number and shape factor H and is originally given by

$$C_f = 0.246\ Re_{\theta_{ss}}^{-0.268}\ \exp(-1.56\ H) \tag{D.18}$$

where $Re(\theta_{ss})$ is defined through

$$Re_{\theta_{ss}} = \frac{\hat{w}_s \theta_{ss}}{\nu} \tag{D.19}$$

As for the entrainment rate, Sumner and Shanebrook [19] analysed compressibility effects on skin friction and showed the validity of the following equation

$$C_f = 0.246\ Re_{\theta_{ss}}^{-0.268} \left(\frac{T_e}{T^*} \right) \exp(-1.56\ H\ ) \tag{D.20}$$

where Eckert's reference temperature T* and the kinematic shape factor H are introduced. The reference temperature T* for adiabatic walls is given by

$$\frac{T^*}{T_e} = 1 + 0.72\ r\ \frac{\gamma-1}{2}\ M_e^2 \tag{D.21}$$

where r is the recovery factor.

Experiments show that the effect of curvature on the skin friction is not to be neglected. These experiments however indicate that the Ludwig-Tillman equation eq (D.20) is still valid. For different types of curved boundary layer flows the increase in friction and in shape factor due to curvature are related by

$$\frac{dC_f}{C_f} = -\ 2.5\ \frac{dH}{H} \tag{D.22}$$

This behaviour is correctly predicted by the Ludwig-Tillman correlation, since from eq (D.20) it follows that

$$\frac{dC_f}{C_f} = -\ 1.56\ H\ \frac{dH}{H} \tag{D.23}$$

Eqs (D.22) and (D.23) are practically equivalent for current values of H.

D.4 Profile models

Velocity profiles are introduced in order to close the system of equations. Velocity profiles and boundary layer thicknesses have been defined in meridional coordinates (figure D.2). In this way, the orthogonality of the basic equations is conserved and all the curvature, coriolis and centrifugal contributions are found in a simple way. In analogy with the EWBL profile models (section 4), following model equations are introduced :

$$\frac{w_s}{w_s^*} = 1 - b\left(1 - \frac{u}{\delta}\right)^n \tag{D.24}$$

$$\frac{w_n - w_s \mathrm{tg}\alpha}{w_s^*} = (1-b)\mathrm{tg}\varepsilon'_w \left(1 - \frac{u}{\delta}\right)^n \tag{D.25}$$

where s lines are the projection of streamlines on an axisymmetric stream surface and where n lines are normal to it.
The parameters b and n are correlated through the following relation [2,3]

$$b = e^{-10n\sqrt{C_f}} \tag{D.26}$$

The introduction of the model equations in the different thicknesses is detailed in (De Ruyck and Hirsch, 1987, first interim report).

Solution procedure

The following differential equations are considered :

(i) the meridional momentum equation (D.8)
(ii) the radial momentum equation (D.9)
(iii) the entrainment equation (D.14)

Extra relations are

(i) the entrainment rate equation (D.16)
(ii) the friction law equation (D.18)

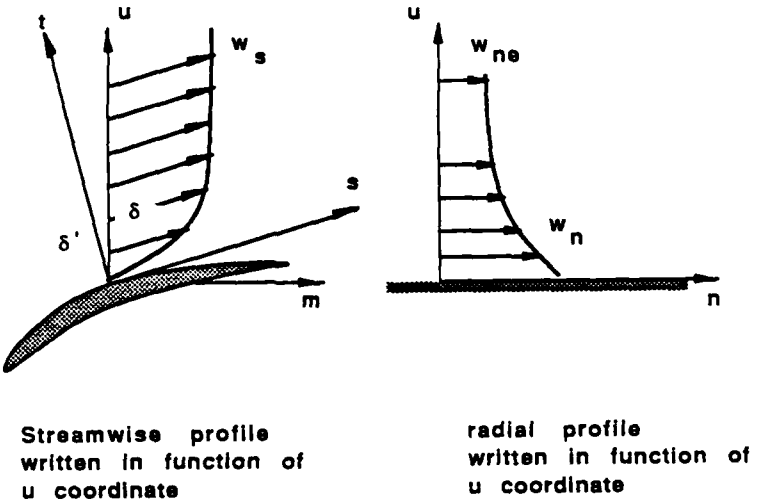

Streamwise profile written in function of u coordinate

radial profile written in function of u coordinate

figure D.2 : profile boundary layer velocity profiles

(iii) the profile model equations (D.24) and (D.25), applied in the definitions (D.4) to (D.7)

Radial momentum and displacement thicknesses are obtained, from which radial profiles can be reconstructed through the radial velocity model equation (D.7).

APPENDIX E : LOCAL WAKE MOMENTUM EQUATIONS

The decay of the center wake velocity is determined from the center wake momentum equation which can be written as

$$\hat{\rho}(\vec{\hat{W}}.\vec{\nabla})\vec{\hat{W}} - \rho(\vec{W}.\vec{\nabla})\vec{W} + 2\vec{\omega}\Lambda(\hat{\rho}\vec{\hat{W}}-\rho\vec{W}) = -\vec{\nabla}(\hat{p}-p) + \vec{\nabla}(-\bar{\bar{\tau}}) \tag{E.1}$$

Assuming w_n small and $\partial_u w_m = 0$ at the wake center, the meridional component can be found from (see appendix D)

$$\vec{e}_m.(\vec{W}.\vec{\nabla})\vec{W} = w_m \frac{\partial w_m}{\partial m} + w_u \frac{\partial w_m}{\partial m} + w_u \left(\frac{w_u}{R_{um}} - \frac{w_m}{R_{mu}} \right)$$

$$= w_m \frac{\partial w_m}{\partial m} + \frac{w_u^2}{R_{um}} \tag{E.2}$$

$$\vec{e}_m.2\vec{\omega}\Lambda\rho\vec{W} = \pm 2\omega \frac{r}{R_{um}} \rho w_u \tag{E.3}$$

$$\vec{e}_m.\vec{\nabla}\bar{\bar{\tau}} = \frac{\rho\nu}{\delta^2} \frac{\partial^2}{\partial\eta^2} w_m \tag{E.4}$$

Using eqs (E.2) to (E.4), equation (E.1) reduces to

$$\hat{w}_m \frac{\partial \hat{w}_m}{\partial m} - w_m \frac{\partial w_m}{\partial m} + (\hat{w}_u - w_u) \frac{1}{R_{um}} \left[(\hat{w}_u + w_u) + 2U \right] = -\frac{\nu}{\delta^2} \frac{\partial^2}{\partial\eta^2} w_m \tag{E.5}$$

Applying eq (9.1), and neglecting the curvature term for a while, one can find, for η=0 at pressure side

$$\hat{w}_m \bar{b}(2-\bar{b}) \frac{\partial \hat{w}_m}{\partial m} + \hat{w}_m^2(1-\bar{b}) \frac{\partial \bar{b}}{\partial m} = \hat{w}_m \frac{\nu}{\delta^{+2}} \left(b^+ f_0'' + (\bar{b}-b^+) g_0'' \right) \tag{E.6}$$

The term in g"(0) gives a discontinuity in the second derivative when going from pressure to suction side. Taking the average over both sides and equation (9.3) for f $\left(f''(0)=-12\right)$ one can write, for $\bar{b}$

$$\frac{1}{\bar{b}}\frac{\partial \bar{b}}{\partial m} = -\frac{12\nu}{(1-\bar{b})\bar{\delta}^2 w_m} - \frac{(2-\bar{b})}{(1-\bar{b})}\frac{1}{w_m}\frac{\partial \hat{w}_m}{\partial m} \tag{E.7}$$

where a mean value for δ is defined as

$$\frac{1}{\bar{\delta}^2} = \frac{1}{2\bar{b}}\left(\frac{b^+}{\delta^{+2}} + \frac{b^-}{\delta^{-2}}\right) \tag{E.8}$$

Expressing the momentum equation (E.1) in η=0, only one equation is obtained for both sides. This equation describes the mean wake velocity defect.

In order to obtain more information about pressure and suction side mixing, a relation is searched between b^+ and b^-. This relation is obtained by writing eq (E.1) in η_1, where η_1 is such that

$$1 = f_1 >> g_1 \tag{E.9}$$

η_1 is a point close to the wake center but which is not influenced by the other wake side. In this way, eq (E.1) reduces to, for the pressure side and suction side

$$\begin{aligned}
\hat{w}_m b^+(2-b^+)\frac{\partial \hat{w}_m}{\partial m} + \hat{w}_m^2(1-b^+)\frac{\partial b^+}{\partial m} &= \hat{w}_m \frac{\nu}{\delta^2}\left(b^+ f_1'' + (\bar{b}-b^+) g_1''\right) \\
\hat{w}_m b^-(2-b^-)\frac{\partial \hat{w}_m}{\partial m} + \hat{w}_m^2(1-b^-)\frac{\partial b^-}{\partial m} &= \hat{w}_m \frac{\nu}{\delta^2}\left(b^- f_1'' + (\bar{b}-b^-) g_1''\right)
\end{aligned} \tag{E.10}$$

and, taking the difference, with $\Delta b = b^+ - b^-$

$$\hat{w}_m 2(1-\bar{b})\,\Delta b\frac{\partial \hat{w}_m}{\partial m} + \hat{w}_m^2(1-\bar{b})\frac{\partial \Delta b}{\partial m} - \hat{w}_m^2\,\Delta b\frac{\partial \bar{b}}{\partial m} = \hat{w}_m \frac{\nu}{\delta^2}\Delta b\,(f_1'' - g_1'') \tag{E.11}$$

Hence,

$$\frac{\partial \Delta b}{\partial m} = -\frac{\nu \Delta b}{\delta^2 w_m(1-b)}(g_1'' - f_1'') + \frac{\Delta b}{(1-b)}\frac{\partial \bar{b}}{\partial m} - 2\Delta b\frac{1}{w_m}\frac{\partial \hat{w}_m}{\partial m} \tag{E.12}$$

and taking eqs (9.3) and (9.4) for f and g yields, with eq (E.9)

$$\frac{1}{\Delta b}\frac{\partial \Delta b}{\partial m} = -\frac{12\,\nu}{\delta^2 \hat{w}_m (1-\bar{b})} + \frac{1}{(1-\bar{b})}\frac{\partial \bar{b}}{\partial m} - \frac{2}{\hat{w}_m}\frac{\partial \hat{w}_m}{\partial m} \qquad (E.13)$$

In a very similar way, by considering the projection of eq (E.1) in the n direction, one can find

$$\frac{1}{\Delta(tg\alpha+tg\varepsilon)}\frac{\partial}{\partial m}\Delta(tg\alpha+tg\varepsilon) = -\frac{12\nu}{\delta^2 \hat{w}_s (1-\bar{b})} - \frac{1}{\hat{w}_s}\frac{\partial \hat{w}_s}{\partial m} \qquad (E.14)$$

Eqs (E.13) and (E.14) close the system of wake equations, the only unknown left is the eddy viscosity coefficient ν which is obtained from

$$\nu = K\delta b \hat{w}_m \qquad (E.15)$$

The coefficient K is to be calibrated.


DAT
FILM
8

$$\frac{T^*}{T} = 1 + 0.72\ a$$